Side chain interactions at the dimer interface of *Vibrio* alkaline phosphatase determine its reactivity, stability and desthiobiotin inhibition

Sigríður Stefanía Hlynsdóttir

Faculty of Physical Sciences
University of Iceland
2018

Side chain interactions at the dimer interface of *Vibrio* alkaline phosphatase determine its reactivity, stability and desthiobiotin inhibition

Sigríður Stefanía Hlynsdóttir

15 ECTS thesis submitted in partial fulfilment of a *Baccalaureus Scientiarum* degree in biochemistry

Advisor
Bjarni Ásgeirsson

Co-advisor
Magnús Már Kristjánsson

Faculty of Physical Sciences
School of Engineering and Natural Sciences
University of Iceland
Reykjavik, May 2018

Side chain interactions at the dimer interface of *Vibrio* alkaline phosphatase determine its reactivity, stability and inhibition by desthiobiotin
15 ECTS thesis submitted in partial fulfilment of a *Baccalaureus Scientiarum* degree in biochemistry

Faculty of Physical Sciences
School of Engineering and Natural Sciences
University of Iceland
Dunhagi 3
107 Reykjavik

Telephone: 525 4000

Bibliographic information:
Sigríður Stefanía Hlynsdóttir, 2018, *Side chain interactions at the dimer interface of* Vibrio *alkaline phosphatase determine its reactivity, stability and desthiobiotin inhibition*, B.Sc. thesis, Faculty of Physical Sciences, University of Iceland, 71 bls.

Reykjavik, May 2018

Abstract

Vibrio alkaline phosphatase (VAP) is a homodimeric, psychrophilic enzyme. A homodimer is, by far, the most dominant quaternary enzyme structure found in nature. It is therefore obvious that this particular structure gives the enzymes some advantage in the evolutionary race. Many suggestions have been proposed, from stabilization effects due to a smaller surface to volume ratio, an increased ratio of active sites to surface and more recently, the idea of "cross-talking" between subunits where only one active site has catalytic capabilities at any given time.

In this study, the enzyme was mutated to try and disrupt the dimer equilibrium. A few methods are being developed to assess this equilibrium and three of them were used for this study. CD spectroscopy monitors a change in the enzymes circular dichroism due to changes in its secondary structure. Fluorescence spectroscopy detects a change in the environment of Trp residues that cause a shift in λ_{max} when the protein is denatured. Dilution induced dimer dissociation to monomers on the grounds of Le Chatelier's principle. Previous studies have shown that VAP unfolding involves at least two intermediate states, one with an inactive dimer and one with unfolded monomers, before the enzyme is completely denatured, $N_2 \rightarrow I_2 \rightarrow 2I \rightarrow 2D$.

This study also assessed a possible inhibition of desthiobiotin (DDB) on VAP. DDB is used to elute purified enzyme samples of *Strep*-Tactin® affinity columns. Recently, crystal images of VAP in a solution containing DDB revealed some kind of interaction between the molecule and residues close to the active site. Results revealed inhibitory effect ($K_i = 0.091$) at 0.25 mM DDB a 10-fold dilution compared to the concentration used for elution of purified enzymes. The exact characteristics of this inhibition are still unclear, but it is likely of a mixed noncompetitive nature.

Útdráttur

Alkalískur fosfatasi úr *Vibrio* (VAP) er kuldaaðlagað ensím sem myndar einsleita tvíliðu. Einsleitar tvíliður eru lang algengasta 4. stigs bygging ensíma í náttúrunni. Það er því augljóst að þessi ákveðna bygging gefur ensímum einhvers konar yfirburði fram yfir aðrar byggingar þegar kemur að þróun lífs. Margar tilgátur hafa verið lagðar fram um hvað það er sem gefur einsleitum tvíliðum þetta forskot. Allt frá stöðgandi hrifum vegna minna hlutfalls yfirborðs miðað við rúmmál og auknu hlutfalli hvarfstöðva miðað við yfirborð. Nýlega hafa komið fram hugmyndir um ”samtöl” milli undireininganna þar sem aðeins önnur hvarfstöðin hefur að bera hvötunargetu á hverju gefnu augnabliki.

Í þessu verkefni var ensímið stökkbreytt með von um að raska tvíliðu jafnvæginu. Nokkrar aðferðir eru í þróun til að meta þetta jafnvægi og voru þrjár notaðar í þessu verkefni. Hringskautsmælingar fylgjast með breytingum í gleypni snúins ljóss sem verða vegna breyting í annars stigs byggingu ensímsins. Sundrun tvíliða í einliður við ensím þynningu byggt á lögmáli Le Chatelier. Fyrri rannsóknir hafa sýnt að afmyndun VAP felur í sér a.m.k. tvö millistigs ástönd, óvirka tvíliðu og svipmyndaðar einliður, áður en próteinið afmyndast algjörlega, $N_2 \rightarrow I_2 \rightarrow 2I \rightarrow 2D$.

Verkefnið fól einnig í sér að meta mögulega hindrun desthiobiotin (DDB) á VAP. DDB er notað til að losa einangrað einsím af sértækri *Strep*-Tactin® skilju. Nýlega hafa kristallamyndir af VAP, í lausn með DDB, sýnt að sameindin binst einhvern veginn við ensímið, við amínósýruleifar nálægt hvarfstöðinni. Niðurstöðurnar sýndu fram á hindrun ($K_i = 0{,}091$) við 0,25 mM DDB, 10-falda þynningu m.v. styrk DDB sem notaður er til að losa ensím af súlunni. Nákvæmir eiginleikar hindrunarinnar eru enn óskýrir en hindurnin er líklega af svokallaðri „mixed noncompetitive“ gerð.

Contents

List of Figures

List of Tables

Abbreviations

AP	Alkaline phosphatase
Caps	3-(Cyclohexylamino)-1-propanesulfonic acid
CBBG	Coomassie Brilliant Blue G-250
CD	Circular dichroism
DDB	d-Desthiobiotin
DEA	Diethanolamine
E•P	Enzyme-Product complex
E•S	Enzyme-Substrate complex
IPTG	Isopropyl β-D-1-thiogalactopyranoside
Mops	3-Morpholinopropane-1-sulfonic acid
***p*NPP**	*p*-Nitrophenyl phosphate
TMC	Tris-Magnesium-Chloride
Tris	2-Amino-2-(hydroxymethyl)-1,3-propanediol
VAP	*Vibrio* alkaline phosphatase

Acknowledgements

First, I want to thank my advisor, Prof. Bjarni Ásgeirsson, for giving me the opportunity to work on this project and for his guidance over the past year. I also want to thank my fellow lab partners for their help, guidance and good talks. I especially want to thank Jens G. Hjörleifsson, for without him I would not have been able to finish all that I accomplished these past months. I also want to thank all my family, for their support and countless babysitting hours over the past three years. And finally, I want to thank my fellow students for all the great times we've had together.

1 Introduction

1.1 Enzyme kinetics

Enzyme kinetics is one of the central studies of biochemistry. It is the study of how enzymes catalyze chemical reactions. Enzymes are under constant evolutionary pressure. By studying enzyme kinetics, we are able to get a better understanding of how species might have evolved to adapt to extremely different environments. By studying one enzyme, we might also shed a light on how homologous enzyme function. This chapter will start by describing the basic principles behind the study of enzyme kinetics.

Figure 1 shows a simple scheme for an enzyme-catalyzed reaction. A substrate molecule binds to the enzyme to form an enzyme-substrate complex, $E \bullet S$, also called a Michaelis-Menten complex. The catalytic reaction takes place and the enzyme is left bound to the product, $E \bullet P$. Finally, the product is released [1].

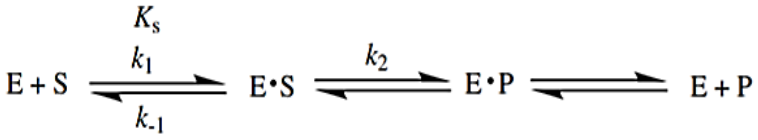

Figure 1. A simple scheme for an enzyme-catalysed reaction.
The simplest form of enzymatic catalysis involves a single enzyme and a single substrate molecule. The substrate (S) binds to the enzyme (E) and is catalysed to form product (P). Subsequently, the product is released, and the enzyme is again available for catalysis. The Michaelis-Menten *equation (Eq. 1) is used to describe the rate of this enzyme-catalysed reaction. Picture taken from* [1].

The **Michaelis-Menten equation** (Eq. 1) is used to describe the rate of this simple single-substrate enzyme-catalyzed reaction. The **Michaelis-Menten constant**, K_m, is dependent on the rate constants of the individual steps, $K_m = (k_{-1} + k_2)/k_1$. When the reaction rate is exactly one-half of the enzymes maximal rate, i.e. $v_0 = \frac{1}{2}V_{max}$, K_m is equal to $[S]$ (Eq. 2) [2].

$$v_0 = \frac{V_{max}[S]}{K_m + [S]} \qquad Eq.1$$

$$\frac{V_{max}}{2} = \frac{V_{max}[S]}{K_m + [S]} \Leftrightarrow K_m = [S] \qquad Eq.2$$

A derivative of the Michaelis-Menten equation can be used to describe a multitude of enzymes said to follow **Michaelis-Menten kinetics** (Eq. 3). The turnover number, k_{cat}, represents the maximum number of substrate molecules a single catalytic site is able to convert to a product per active site in a given unit of time. The value of k_{cat} can vary greatly and span a range of at least 9 orders of magnitude. However, it's value is never higher than then the single slowest rate constant for a given multi-step reaction. Still, enzyme catalysis has two other important steps that affect the reaction rate, substrate binding and product release.

$$v_0 = \frac{k_{cat}[E_t][S]}{K_m + [S]} \qquad Eq.3$$

A way to compare the catalytic efficiency of enzymes is to look at their **specificity constant**, defined as k_{cat}/K_m. A "perfect" enzyme is an enzyme whose rate limit is set by diffusion of molecules in the solvent. The specificity constant for said enzyme would be between 10^8 – 10^9 $s^{-1}M^{-1}$. This limit means that an enzyme with a high turnover number would also have to have a relatively high value of K_m and, therefore, need a higher substrate concentration to reach V_{max} [1,2]. A study of ~ 5000 unique natural enzyme-substrate reactions concluded that most enzymes have a k_{cat} value between 1 – 100 s^{-1} and a k_{cat}/K_m value between 10^3 – 10^6 $s^{-1}M^{-1}$. It also showed that enzymes of central metabolic pathways have higher turnover numbers (~ 30-fold higher) and higher specificity constants (~ 6-fold higher) than enzymes of secondary metabolism reactions [3].

Michaelis-Menten kinetics can also be applied to multi-substrate enzymes if the concentrations of all but one substrate are kept high and constant throughout the assay. Results from such assays can e.g. indicate whether the reaction follows a sequential mechanism – a product is released only after all substrates are bound – or a ping-pong mechanism– a product is released before all substrates are bound to the enzyme [4].

1.2 Alkaline Phosphatase

Alkaline phosphatase (AP) is ubiquitous in nature, found both in prokaryotes and eukaryotes, in man as well as *Escherichia coli*. The enzyme facilitates phosphoryl transfer by catalyzing the hydrolysis of phosphate monoesters. Transfer of phosphoryl groups is one of the main chemical reactions that take place in organisms. More precisely, it is the hydrolysis of phosphate esters that is in large part responsible for numerous biological processes such as biological signals, transfer of energy and protein synthesis. Uncatalyzed, the reaction is extremely slow, with the half-time for attack of water in the trillions of years at 25°C (k = 2 x 10^{-20} s^{-1}). Alkaline phosphatase from *E. coli* has been shown to enhance the rate of

hydrolysis at room temperature by a factor of $\sim 10^{21}$, making it one of the most proficient enzymes identified [5–7].

Although similarities in amino acid composition between different APs are minimal – the sequence alignment between bacterial and mammalian variants are 25-30% identical – the amino acid sequence around the active site is surprisingly well conserved. Secondary and tertiary structures are also highly similar. Different variants of AP seem to all have the same core structure and variations are mostly away from the active site [8].

AP is usually a homodimeric metalloenzyme with a typical α/β structure. Each subunit consists of a central β-sheet surrounded with 15 helices of various lengths, with three metal binding sites [8,9]. The key residues of the active site are Asp101, Ser102, Ala103 and Arg166 as well as the three metal ions (two Zn^{2+} and one Mg^{2+}). Both zinc ions bind to the phosphate group of the substrate/product. One of the zinc ions, as well as the magnesium ion, also participates in activating the Ser102 residue [8,10,11]. Figure 2 shows the reaction mechanism of the hydrolysis and transphosphorylation catalyzed by APs. Once the Ser102 residue has been activated as a nucleophile, it is temporarily phosphorylated, resulting in a covalent phosphoryl intermediate, $E-P$. In the absence of a phosphate acceptor, the intermediate is hydrolyzed and the product, an inorganic phosphate group (P_i), is subsequently released. If a phosphate acceptor is available, the enzymes transfers the phosphoryl group onto the phosphate acceptor giving a new phosphate ester, R_2OP [12].

1.3 *Vibrio* alkaline phosphatase

The alkaline phosphatase of this study (VAP) comes from the psychrophilic bacteria *Vibrio splendidus*. The *V. splendidus* strain, G15-21, was isolated from the coastal waters near south-west Iceland. It is a homodimeric enzyme with a molecular mass of 55 kDa for each monomer. The enzyme is cold-adapted and very heat-labile but can be stabilized with NaCl. When stored at room temperature, VAP loses 90% of its activity in 1 day whereas when the enzyme is stored in 0.5 M NaCl the enzyme's activity is preserved for two days and only drops down to 75% of its initial activity after 4 days at room temperature [13,14].

The enzyme consists of two monomers. These monomers are held together weaker than monomers of heat-tolerant APs which explain the enzyme's instability. These weak interactions are also presumably responsible for the enzymes high catalytic activity, preventing it from becoming too rigid at low temperatures. As previously mentioned, most enzymes have a k_{cat} value between 1 and 100 s^{-1} (see section 1.1). At 25°C and pH 10.0, VAP's optimum pH level, the enzyme has a k_{cat} of 350 s^{-1} and at 37°C it has a k_{cat} of 1024 s^{-1}. At 15°C, the enzyme still has a k_{cat} value of 164 s^{-1} [13,15].

VAP is inhibited by inorganic phosphate which acts as a competitive inhibitor of the enzyme with K_i of 1.7 mM [13]. This is comparable to K_i for phosphate inhibition on the cold-active AP from Atlantic cod (K_i of 1.12 mM) but relatively high compared to phosphate inhibition of the mesophilic APs from *E. coli* and *V. cholerae* (K_i of 0.056 mM and 0.032 mM, respectively). Figure 3 describes the reaction scheme of APs. Under non-transphosphorylating condition and pH > 8, the release of inorganic phosphate is the rate limiting step. The enhanced catalytic activity of cold-adapted APs might be due to their

decreased affinity towards the inorganic phosphate. It is possible that the decreased affinity is the result of increased flexibility which might facilitate release of phosphate product [13,16]. The increased activity might also be due to weaker interactions between the monomers [15]. Weakened monomer interactions have been suggested as a key adaptation of psychrophilic enzymes to compensate for the decrease in chemical reaction that inevitably follows temperature decrease [17].

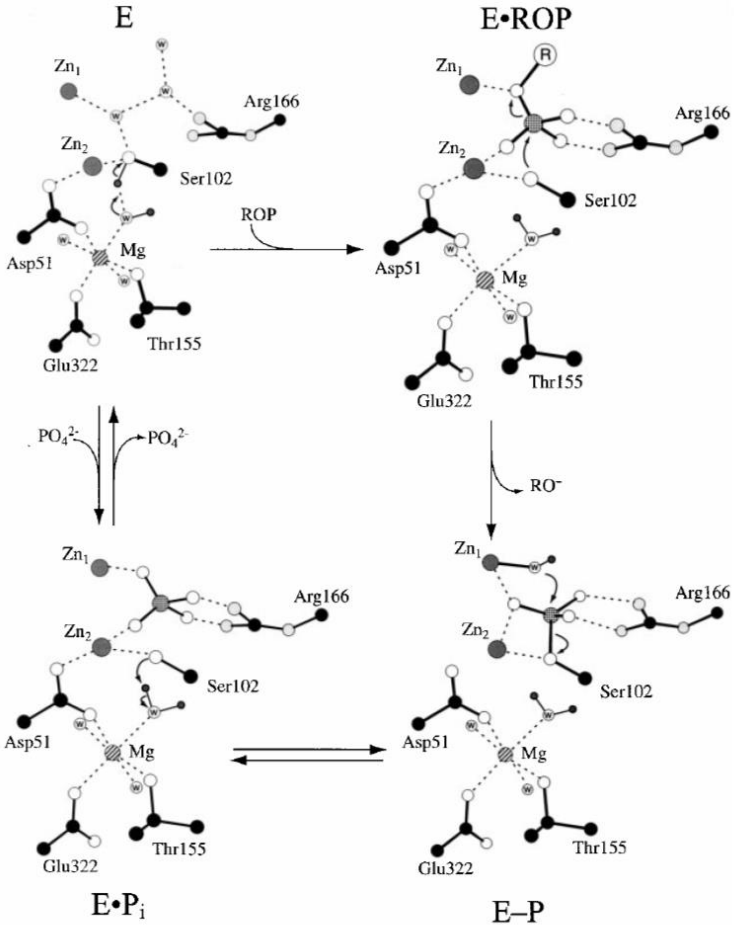

Figure 2. The reaction mechanism of phosphate hydrolysis catalysed by alkaline phosphatase.

Ser102 participates in a hydrogen bond with a Mg-coordinated hydroxide ion at the phosphate-binding site. The ester oxygen atom of the substrate's phosphate group is coordinated to one of the zinc ions, Zn1. Other oxygen atoms of the phosphate interact with Arg166 and the other zinc ion, Zn2. Next, the Mg-coordinated hydroxide ion deprotonates Ser102, activating it as a nucleophile. The activated serine residue attacks the phosphorous atom in a nucleophilic Sn2 reaction, breaking the ester bond. This results in a covalent enzyme-phosphate intermediate. A Zn1-coordinated hydroxide ion attacks the phosphorous atom in another nucleophilic Sn2 reaction, breaking the covalent enzyme-phosphate bond. Finally, the Mg-coordinated water molecule acts as a general acid, donating a proton to Ser102. Picture taken from [11].

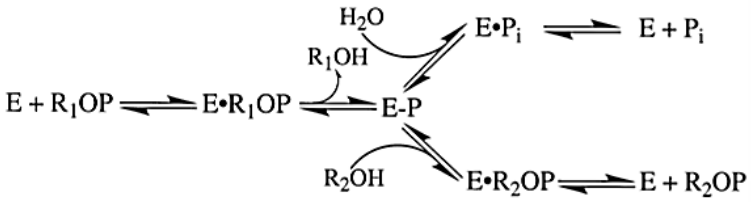

Figure 3. Reaction scheme of hydrolysis and transphosphorylation catalysed by alkaline phosphatases.
The substrates phosphate group binds to the enzyme. Under non-transphosphorylating conditions and pH > 8, the release of the inorganic phosphate is the rate limiting step. The enhanced catalytic activity of cold-adapted alkaline phosphatases might be due to their decreased affinity towards inorganic phosphate, compared to their mesophilic homologues. [13,16]. *Picture taken from* [12].

1.4 Enzyme inhibition

Enzymes are macromolecules that catalyze reactions of biological systems that otherwise would take far too long to sustain life. Since enzymes play an important part in nearly all cellular processes, it is crucial for the cell to be able to control their activity. One way to influence enzyme activity is by inhibitors, molecules that interfere with catalysis. Inhibitors are roughly categorized into two groups: Reversible and irreversible inhibitors [2]. Table 1.1 shows further categorization of enzyme inhibitors.

Table 1.1. Categorization of enzyme inhibitors.

Reversible inhibitors	Competitive inhibitors
	Uncompetitive inhibitors
	Non-competitive inhibitors
	Substrate inhibition
Irreversible inhibitors	Covalently bound inhibitors
	Mechanism-based inhibitors

1.4.1 Reversible inhibitors

Reversible inhibitors hinder the enzyme temporarily. The inhibitors can bind to the active site of an enzyme or they can bind allosterically, inducing conformational changes in the enzyme that either decrease its affinity for the substrate or reduce its catalytic abilities. For multi-substrate enzymes, it is not uncommon for an inhibitor to bind to the same site as one substrate and be an allosteric inhibitor for another substrate. Inhibitors can also show partial inhibition where the enzyme retains some of it catalytic abilities [1].

Competitive inhibitors, as the name suggests, compete with the substrate for the free enzyme to form an enzyme-inhibitor complex, $E \bullet I$. Once the inhibitor is bound to the enzyme, the substrate is unable to bind to it too. Therefore, the presence of a competitive inhibitor in a solution pulls the $E + S \rightleftharpoons E \bullet S$ equilibrium to the left, resulting in an increased value of the Michaelis-Menten constant, K_m. However, if the substrate concentration is sufficiently high, virtually all the enzyme will be present as the $E \bullet S$ complex. Thus, competitive inhibitors do not affect the maximal rate, V_{max}, of the catalytic reaction [1].

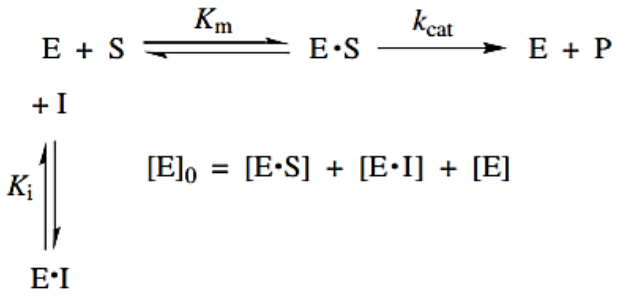

Figure 4. A reaction scheme of competitive enzyme inhibition.
Competitive inhibitors compete with the substrate for the free enzyme. The inhibition can be overcome with higher concentrations of substrate. K_m is decreased while V_{max} is unaffected [1].

Uncompetitive inhibitors bind to the $E \bullet S$ complex giving an enzyme-substrate-inhibitor complex, $E \bullet S \bullet I$. The inhibitor is often allosteric, i.e. it binds to the enzyme away from the active site. When $[S]$ is negligible, so is the amount of $E \bullet S$ complexes, and the inhibitor has minimal effect. However, as the substrate concentration increases, the effects of the inhibitor also increase as the supply of substrate bound enzymes increases. This type of inhibitors affects both the observed value of K_m and V_{max}. The $E + S \rightleftharpoons E \bullet S$ equilibrium is pulled to the right lowering the K_m value. And because a part of the enzyme will be bound in an inactive complex with the inhibitor the value of V_{max} is also lowered.

Uncompetitive inhibition is usually only observed for multi-substrate enzyme reactions but in theory it could also apply to single-substrate reactions. This type of inhibition is thought to be very rare in nature, possibly because it can have an immense effect on metabolic intermediates and affects metabolic pathways to much greater extent than e.g. competitive inhibition [2,18]. L-Phenylalanine inhibition of alkaline phosphatase is one of the few samples of uncompetitive inhibition of a single substrate enzyme [19].

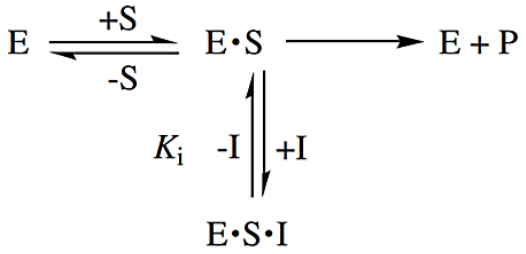

Figure 5. A reaction scheme of uncompetitive enzyme inhibition.
Uncompetitive inhibitors bind only to the E•S complex. The effects of the inhibitor increase with increased substrate concentrations. Uncompetitive inhibition decreases both K_m and V_{max} (Nelson and Cox 2013). Picture taken from (Silverman 2002).

Non-competitive inhibitors bind to both free enzyme and the enzyme-substrate complex. This type of inhibition, like uncompetitive inhibition, is also rare for single-substrate enzymes. However, it is common for multi-substrate enzymes. Figure 6 shows two dissociation constants. K_m for the dissociation of S from $E \bullet S$ and K'_m for the dissociation of S from $E \bullet S \bullet I$. If the two constants are equal the inhibition is a **pure non-competitive inhibition**. The value of K_m is not affected but V_{max} is lowered since some of the enzyme is bound in an inactive complex with the inhibitor. When the two dissociation constants are different the inhibition is called a **mixed inhibition** and shows characteristics of both competitive and uncompetitive inhibition. The substrate can bind to both free enzyme and the $E \bullet I$ complex, but the latter has lower affinity to the substrate. Therefore, K_m is increased while V_{max} is decreased [1].

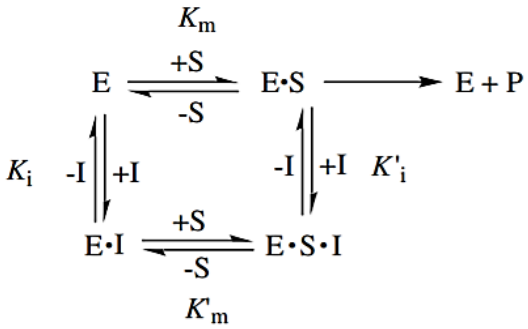

Figure 6. A reaction scheme of non-competitive enzyme inhibition.
Non-competitive inhibitors can bind to both free enzyme and the E•S complex. When the inhibitor exhibits equal affinity towards both forms of enzyme, it is a pure non-competitive inhibitor. If not, the inhibitor is a mixed inhibitor and has characteristics of both competitive and uncompetitive inhibition. A pure non-competitive inhibitor decreases V_{max} but has no effect on K_m. A mixed inhibitor increases K_m and lowers V_{max}[1].

1.4.2 Substrate inhibition

Sometimes, enzyme activity deviates from the Michaelis-Menten model. One of the most common deviations are **substrate inhibitions**. Researchers have disagreed on how common or rare substrate inhibition is under physiological circumstances [20]. However, studies have shown that substrate inhibition can be essential for a number of biological phenomena. Many mechanisms have been proposed to describe substrate inhibition.

One such model describes an ES_2 complex where the second substrate molecule is an allosteric inhibitor of the first one. Figure 7 shows a reaction scheme where a second substrate molecule is an inhibitor. If $k_4 = 0$ the enzyme velocity goes to zero when the substrate concentration is high enough. If the second substrate molecule is only a partial inhibitor the product formation continues but at a reduced rate [21,22].

Another model proposes that the enzyme, after the product is released, has to go through an inactive and non-activatable isomerization step before it can bind to a new substrate molecule. This intermediate state can also bind to a substrate molecule but at low substrate concentration, the isomerization to an activatable state is much faster than the binding of the non-activatable state to the substrate. When substrate concentration is sufficiently high this is no longer true and the enzyme has to go through an additional step, to release the substrate molecule before it can return to the activatable state [20].

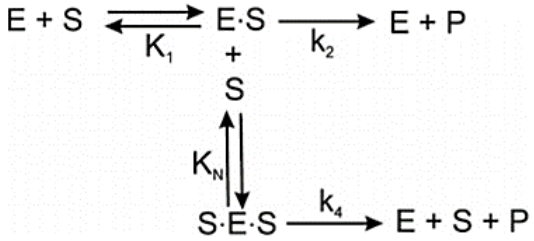

Figure 7. A reaction scheme of enzyme inhibition by substrate.
Enzymes can be inhibited by too high substrate concentration. The second substrate can either inhibit the enzyme completely, decreasing V_{max} to 0, or it can be a partial inhibitor, only reducing V_{max} [22]. *Picture taken from (Silverman 2002).*

1.4.3 Irreversible inhibition

Sometimes inhibitors bind to the enzyme in an irreversible manner. **Irreversible inhibitors** either bind covalently to the enzyme or the noncovalent binding is strong enough so that the

inhibitor rarely dissociates from the enzyme – $K_d < 10^{-8}$ M. Usually, irreversible inhibitors resemble the substrate-product transition state intermediate, but enzymes have evolved to bind most tightly to the reaction intermediate. Irreversible inhibition happens in at least two steps. First, the inhibitor binds reversibly to the enzyme. Then, more slowly, the $E \bullet I$ complex is converted into a covalently bound $E - I$ complex [4].

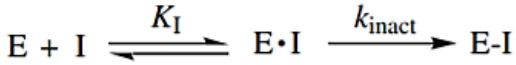

Figure 8. A reaction scheme of irreversible enzyme inhibition.
Irreversible inhibitors either bind covalently to the enzyme or the noncovalent binding is strong enough so that the inhibitor rarely dissociates from the enzyme. The inhibition happens in at least two steps where the inhibitor binds reversibly to the enzyme before it is covalently bound [4]. *Picture taken from (Silverman 2002).*

A special case of irreversible inhibitors are **mechanism-based inactivators** or **suicide inhibitors**. These inhibitors are very specific, and the inhibitors are substrate analogs. The inhibitor binds to the enzyme like the substrate would and the first steps of the catalyzed reaction are carried through, but a product isn't formed and released. Instead, the reaction leads to the formation of a covalent link between the inhibitor and the enzyme [1,2].

1.5 The project

1.5.1 Interactions between the two monomers of VAP

As mentioned before, *Vibrio* alkaline phosphatase is a homodimeric, psychrophilic enzyme. This means the protein adopts a quaternary structure of two identical subunits, or monomers. This particular quaternary structure seems to give enzymes generally a great advantage over other possible configurations. A 1998 study found that only about one fifth of the then identified *E. coli* proteins were monomeric and, of the multimeric proteins, dimers were by far the most common, representing little under 40% of total proteins. The study also found that the vast majority of the proteins were homomeric [23]. Evolution seems to favor multimers over monomers, and homomers over heteromers. But why? What advantage do homomultimers have over other proteins?

When it comes to function and stability, large proteins have many advantages over smaller ones. Larger proteins have relatively smaller surface areas and a higher number of internal interactions. Therefore, the protein can be held stable by numerous weaker intramolecular forces rather than stronger, more rigid, forces. Smaller surface area also means increased entropy of the solvent since fewer molecules are involved in forming a

"cage" around the protein. By constructing large proteins as oligomers, error control in synthesis and regulation of assembly are made simpler, and coding is more efficient [23]. Oligomerization has also been suggested as an adaptation of psychrophilic enzymes. An enzyme with more active sites should have an improved activity compared to homologues with fewer active sites [17].

Many homodimeric enzymes exhibit half-of-site reactivity, where only one-half of the subunits is active at any given time. A previous study of the structure of VAP showed asymmetry between the subunits. The two subunits were shown to vary in flexibility in regions close to the active sites (Figure 9), possibly due to intermolecular interactions between the monomers [15].

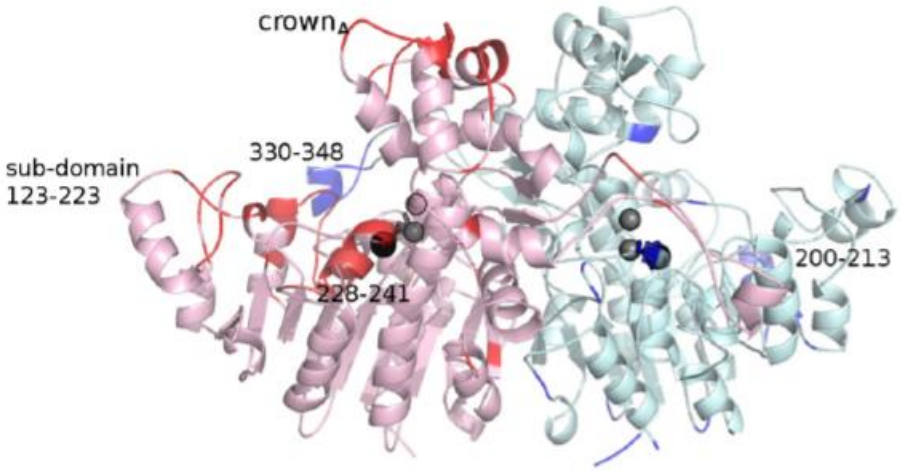

Figure 9. VAP monomers are asymmetric in flexibility in regions close to the active sites.

The figure shows the two subunits of VAP. Monomer A and B are shown as pink and pale-cyan, respectively. Regions of the highest flexibility of monomer A are B are shown in red and blue, respectively. Picture taken from [15].

The aim of this project was to assess the dimer equilibrium and hopefully shed some light on the monomer interactions. The sequence I_{458}VWGTG forms a loop in a site corresponding to where a mutation of Asn in the human tissue-nonspecific AP prevents dimerization [24]. For this study, amino acids in this loop were mutated to try and disrupt the dimer equilibrium. Kinetic parameters of the mutants G461A and W460I were determined with activity measurements. Their resistance to urea and temperature was used to determine their stability. The dimer-monomer equilibrium of mutant G461A was assessed by diluting the enzyme sample until activity decreased. Figure 11 shows where the mutated amino acids are situated.

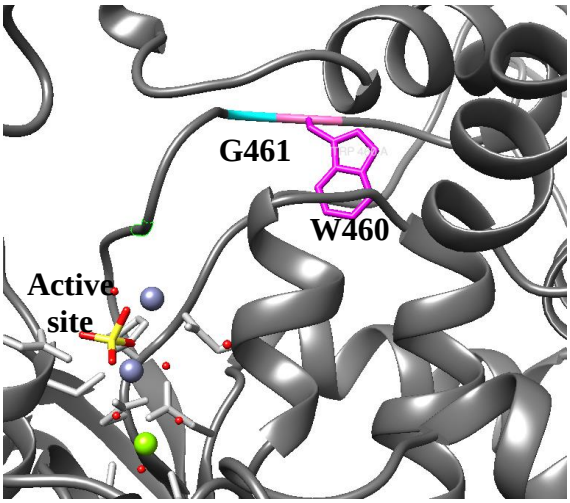

Figure 10. Residues W460 and G461 are situated close to the active site of VAP. *Mutations of residues* ***W460*** *(shown in magenta) and* ***G461*** *(shown in cyan) were analysed in this study. Both residues are situated on a loop close to the active site. The active site is shown with the three metal ions and residues involved in ion binding. W460I and G461A mutations were studied. (The image was created in UCSF Chimera) .*

1.5.2 Desthiobiotin as an inhibitor of VAP

The laboratory group has been using *Strep*-Tactin® affinity columns to purify VAP from enzyme expression cultures for studying its characteristics. The method uses *Strep*-tag II, a small-affinity peptide fused with the protein of interest. The peptide exhibits intrinsic affinity toward core streptavidin, can withstand mild detergents, is resistant to cellular proteases and has almost no biochemical effect. Meanwhile, core streptavidin is highly stable, exhibits low nonspecific interactions and can be used in various forms. Core streptavidin shows high affinity towards d-biotin and binds reversibly to the molecule, so that it (or it derivative with less strong affinity) can be used to elute the purified protein and the resin can subsequently be regenerated [25].

The group has been using desthiobiotin (DDB) to elute VAP from the columns so that the purified enzyme samples contain 2.5 mM DDB. It should be noted that for most measurements, the samples are diluted (by a factor of at least 1000) or dialyzed. Recently, a crystal structure of a sample containing DDB showed that the molecule might be an inhibitor of the enzyme (Figure 11). The molecule seemed to bind to W274, a residue close to the enzyme's active site (see also Figure 32). The aim of the project was to confirm the inhibition of DDB on VAP and characterize it. To do that, the activity of wild-type VAP was measured under different conditions with and without DDB.

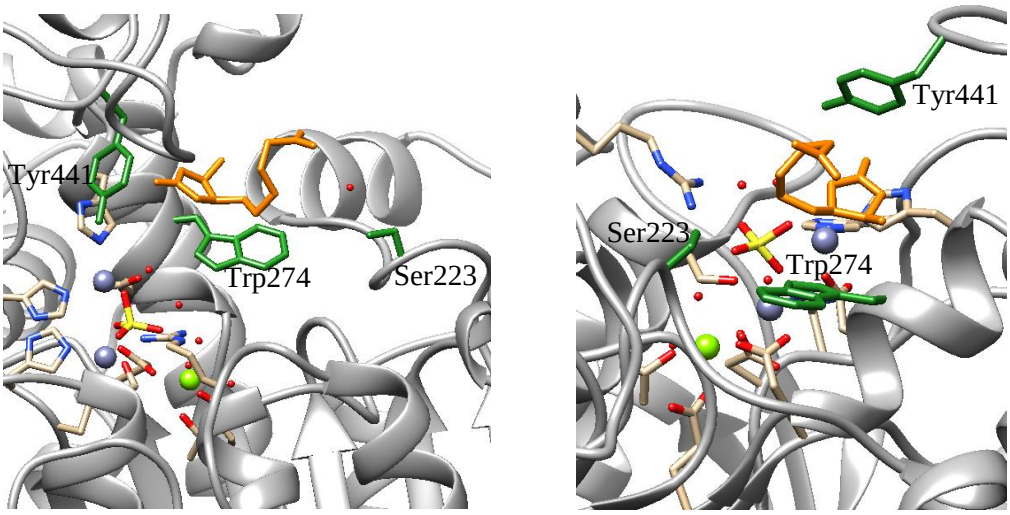

Figure 11. d-Desthiobiotin interacts with residues close to the active site.
Recently, a crystal structure of VAP, crystallised from a solution with DDB, showed the molecule interact with residues close to the active site. The figures show two different angles of the same crystal structure (see also Figure 32*). DDB is shown as orange. Residues it might act with are shown in green (Ser223, Trp 274 and Tyr441). Notice the oxygen coordinated between DDB and Ser223. (The image was created in UCSF Chimera).*

2 Methods and Materials

Following is the description of materials and methods used for this study. Detailed descriptions of the buffers can be found in Appendix A.

2.1 Materials

Materials were generally purchased from Sigma-Aldrich (St. Lois, USA) or Thermo Fisher Scientific (Carlsbad, USA) unless otherwise specified. Primers were purchased from Tag Copenhagen A/S (Denmark). *E. coli* XL10 Gold® Ultracompetent cells were purchased from Agilent Technologies. Lemo21(D3) competent *E. coli* cells and materials for QuikChange® mutagenesis were purchased from New England BioLabs® Inc. Bacto™ Tryptone and Bacto™ Yeast extract were purchased from Becton, Dickinson and Company (Sparks, USA). L(+)-Rhamnose 1-hydrate and Isopropyl β-D-1-thiogalactopyranoside (IPTG) was purchased from AppliChem GmbH (Darmstadt, Germany). desthiobiotin and materials for *Strep*-Tactin® affinity chromatography were purchased from IBA GmbH (Göttingen, Germany). Precasted NuPage™ 4-12% Bis-Tris gels and NuPage™ LDS Sample buffer [4x] were purchased from Invitrogen (Thermo Fisher Scientific, Carlsbad, USA).

2.2 Preparation of mutated plasmids

A total of five mutants were prepared – W460I, G461A, G461S, T462A, T462S. Plasmids for all five mutants were prepared and purified. Jens G. Hjörleifsson designed the primers which were ordered from Tag Copenhagen A/S (Denmark).

2.2.1 Site-directed mutagenesis

The mutated plasmids were prepared using QuikChange site-directed mutagenesis, composed of four steps. Step 1, samples are prepared according to Table 2.1. Next, 0.2 µl of Phusion HF are added to each sample and they mixed using a table-top centrifuge for few seconds. Step 2, the samples are subjected to PCR (GeneAmp® PCR System 2700, Applied BioSystems. The cycling parameters can be seen in 2.2. *Step 3*, the samples are digested with 0.5 µl *Dpn1* endonuclease for 2 h at 37°C to remove the nonmutated parental plasmid template. *Step 4*, the samples are transformed into *E. coli* XL10-Gold® ultracompetent cells. The cells repair nicks in the mutated plasmids and express it for subsequent purification.

For the W460I variant, two samples were made, one with 20 ng pET11a dsDNA template and one with 50 ng. For all other variants, one sample was made with 50 ng template. For control, samples were prepared without primers.

Table 2.1. Ratios of prepared samples for QuikChange® site-directed mutagenesis.
The materials were mixed together in Eppendorf tubes. 0.2 µl Phusion HF was added to the sample and it mixed using a table-top centrifuge for a few seconds. The recipe listed is for one sample.

5x reaction buffer (Phusion GC)	5 µl
dsDNA template (pET11a)	0.2 µl / 0.5 µl[a]
Forward primer	0.45 µl[b]
Reverse primer	0.45 µl[b]
dNTP mix	1 µl
ddH_2O	x µl[c]
	50 µl

a. The amount of dsDNA template varies between samples. For the W460I variant, 0.2 µl and 0.5 µl were tested (~ 20 and 50 ng, respectively). For other variants, 0.5 µl were used.
b. The concentration of primers can vary. A volume that corresponds to 125 ng should be used (for all variants in this study, 125 ng = 0.45 µl). Primers are not added to a control sample.
c. The volume of ddH_2O varies depending on other materials. The total volume of the sample should be 50 µl.

Table 2.2. PCR cycling parameters for QuikChange® site-directed mutagenesis.
The PCR reaction was performed overnight, the samples were kept at 4°C for approx. 16-18h.

Segment	No. of cycles	Temperature	Time
1	1	95°C	30 seconds
2	18	95°C	30 seconds
		55°C	1 minute
		68°C	6 minutes[a]
3	1	68°C	2 minutes
		4°C	∞

a. This time should be 1 minute/kb of plasmid length. The *p*ET11a plasmid, used in this study, is approx. 5.7 kb.

2.2.2 Transformation of *E. coli* XL10-Gold

The PCR product was transformed into *E. coli* XL10-Gold ultracompetent cells accordingly: The cells were removed from freezer and thawed slowly on ice. Fifty µl of cells were placed in a pre-chilled sterile 2 ml Eppendorf tube, one for each sample. One µl of a PCR product (see section 2.2.1) was added to each cell sample, a total of 6 samples (two samples for the

W460I variant and one sample for other variants). The samples were then kept on ice for 10 minutes. The transformation reaction was heat-pulsed for 90 seconds at 42°C and immediately after, the samples were put on ice for 1 minute. 1 ml SOC medium was added to each tube and the samples were incubated for 1 h at 37°C with shaking. The samples were then centrifuged at 2,000 × g for 5 minutes and most of the supernatant discarded. The pellet was resuspended in the remaining liquid (~ 100 µl) and plated on LB agar plates containing ampicillin (100 µg/ml). The plates were than incubated for 16 – 24 h at 37°C.

2.2.3 Plasmid purification

GeneJET™ Plasmid Miniprep Kit (Thermo Fisher Scientific) was used to purify the plasmids before enzyme expression. For each variant three colonies were chosen, resulting in three samples of purified plasmid for each of the variants. The samples were then subjected to electrophoresis to determine their purity and sequenced to confirm the mutation was present. Before the plasmid purification, transformed cells were incubated in 5 ml LB medium containing ampicillin (100 µg/ml) at 37°C overnight with shaking.

The GeneJET™ plasmid purification protocol is as follows. All steps were performed at room temperature and centrifugation was carried out in a table-top microcentrifuge at 12,000 × g, unless stated otherwise. Purified plasmids were stored at -20°C.

1. The cell culture is centrifuged at 1,700 × g for 10 minutes.
2. The precipitate is resuspended in 250 µl of *Resuspension Solution* by vortexing.
3. The solution is transferred to a sterile Eppendorf tube.
4. 250 µl of *Lysis Solution* are added to the sample and it mixed by inverting the tube 4 – 6 times. The solution becomes viscous and clearer.
   - The sample should not be kept for more than 5 minutes in the unneutralized lysis solution to prevent DNA denaturation
5. 350 µl of *Neutralization Solution* are added to the sample and it mixed by inverting the tube 4 – 6 times.
6. The sample is centrifuged at for 5 minutes.
7. The supernatant is carefully transferred to a GeneJET™ spin column.
8. The sample is centrifuged for 1 minute. The flow-through is discarded.
9. 500 µl of *Wash Solution* are added to the spin column and the sample is centrifuged for 30 – 60 seconds. The flow-through is discarded.
10. Repeat step 9.
11. The sample is centrifuged at for 1 minute to remove residual wash solution. The flow-through is discarded.
12. The spin column is transferred into a sterile Eppendorf tube.
13. 50 µl of *Elution Buffer* is added to the center of the spin column.
14. The sample is incubated for 2 minutes at room temperature.
15. The sample is centrifuged at for 2 minutes. The purified plasmid is in the flow-through.

2.2.4 Agarose gel electrophoresis

Agarose gel electrophoresis was used to assess the purity of the plasmid samples. Fifty ml of 1% (w/v) agarose gel was made by mixing 0.5 g agarose powder in 50 ml TAE buffer. The solution was heated in a microwave to completely dissolve the agarose. 50 µl of ethidium bromide were mixed with the solution after it had cooled down (when the flask was comfortable to hold). A casting tray was placed in an electrophoresis chamber. The solution was poured into the casting tray (with one comb for a row of ten wells at the top) and left to solidify for approx. 10 minutes.

TAE buffer was poured over the solidified gel before the comb was removed. The chamber was filled with TAE buffer until it covered the gel. The samples were prepared by mixing 3 µl of sample with 2 µl TAE buffer and 1 µl coloring agent. For reference, a ladder sample was prepared by mixing 3 µl of ladder with 2 µl TAE buffer and 1 µl coloring agent. The samples and the ladder were loaded to the wells of the gel and the chamber connected to a power source of 75 V for 1 h. The gel was subsequently photographed (Gel Doc™ EZ Imager, Bio-Rad) and analyzed with accompanying software (Image Lab© v5.2.1, Bio-Rad Laboratories)

2.2.5 DNA sequencing

The purified plasmid samples, a total of 12 samples, were sequenced by Genewiz, UK.

2.3 Enzyme expression and purification

Two variants were chosen for further studies. G461A (strain 2) and W460I (strain 3). The enzyme was expressed in Lemo21(DE3) competent *E. coli* cells and purified with *Strep*-Tactin® affinity chromatography. SDS-PAGE was used to assess enzyme purity.

2.3.1 Transformation of Lemo21(DE3) competent *E. coli* cells

Purified plasmids were transformed into Lemo21(DE3) competent *E. coli* cells. Before transformation, the cells were centrifuged at 2,000 × g for 5 minutes at room temperature. The transformation protocol was the same as for transforming the *E. coli* XL10-Gold ultracompetent cells for plasmid expression with small modifications (see section 2.2.2). Next, fifty µl of cells were placed in a pre-chilled sterile 2 ml Eppendorf tube, one for each sample. One µl of purified plasmid (see section 2.2.3) was added to each cell sample, a total of 2 samples. The samples were then kept on ice for 10 minutes. The transformation reaction was heat-pulsed for 90 seconds at 42°C and immediately after, the samples were put on ice for 1 minute. 1.0 ml SOC medium was added to each tube and the samples were incubated for 1 h at 37°C with shaking. The samples were then centrifuged at 2,000 × g for 5 minutes and most the supernatant discarded. The pellet was resuspended in the remaining liquid (~

100 µl) and plated on LB agar plates containing ampicillin (100 µg/ml) and chloramphenicol (30 µg/ml). The plates were then incubated for 16 – 24 h at 37°C.

2.3.2 Enzyme expression

Transformed *E. coli* were cultivated for protein expression. Two 20 ml starter culture were prepared by introducing a single colony from each agar plate (see section 2.3.1) into 20 ml LB medium containing ampicillin (100 µg/ml) and chloramphenicol (30 µg/ml). The starter cultures were incubated with shaking (300 rpm) overnight at 37°C. Subsequently, the starter cultures were diluted into the same medium containing an addition of 0.5 mM L-rhamnose. Two mL of starter culture were added to approx. 330 – 350 ml medium in 1 l Erlenmeyer flasks, a total of 8 – 9 flasks for each sample and incubated at 10°C with shaking (200 rpm) for approx. 8 – 10 h. Then, isopropyl β-D-1-thiogalactopyranoside (IPTG) activator was added to the cultures to a concentration of 400 µM (preferably, the cultures should reach an OD_{600} value between 0.4 and 0.6 before the IPTG addition). The cultures were incubated overnight with shaking (200 rpm) at 10°C before enzyme extraction.

2.3.3 Enzyme extraction and purification

The enzyme expression cultures (see section 2.3.2) were stopped when $OD_{600} \approx 0.5$ and the cell culture medium centrifuged at 10,000 × g for 10 minutes at 4°C (Avanti® J-26 XP centrifuge and JLA-16.250 fixed angle rotor, Beckman Coulter, California). The pellet was resuspended in 100 ml lysis buffer (20 mM Tris, 10 mM MgCl2, 0.01% (w/v) Triton X-100, pH 8.0). 1 mg/ml lysozyme was added to the solution and it incubated at 4°C with gentle swirling for 4 h. The lysate was then quick-frozen under liquid N_2 for later use. The lysate was thawed slowly and incubated with DNAse (1 µg/ml) at 4°C for 1 h. The sample was then centrifuge at 20,000 × g for 30 minutes at 4°C, twice, to obtain a clear lysate.

The enzyme samples were purified using the Schmidt and Skerra's *Strep*-tag method with modifications [25]. *Strep*-Tactin® affinity chromatography column was used to purify the enzyme samples. The column was pre-treated with HABA buffer (2-[4-hydroxyphenylazo] benzoic acid) until it became bright-red. HABA washes away any lingering desthiobiotin from previous purifications. Next, the column was equilibrated in TMC binding buffer (20 mM Tris, 10 mM $MgCl_2$, pH 8.0) until it became white. The flow-rate was adjusted to 1.5 ml/min. The clear cell lysate was added to the column and which was subsequently washed with TMC buffer. When measurements of the absorbance at 280 nm (A_{280}) of the flow-through showed the column had reached equilibrium, i.e. when A_{280} values reached the baseline, the column was washed with washing buffer (TMC + 0.15 M NaCl) to elute any nonspecific proteins bound by electrostatic interactions. When the column had reached equilibrium again, the bound enzyme was eluted with elution buffer (TMC + 0.15 M NaCl + 2.5 mM desthiobiotin).

Purified enzyme was collected in 1.0 or 1.5 ml fractions into Eppendorf tubes. Activity of selected fractions was measured with the standard activity assay (see section 2.5.1), most

of them close to the active peak. For the G461A mutant, absorbance of selected fractions at 280 nm was also measured (see section 2.4). Samples of the lysate, and the NaCl eluate were also measured for activity and protein concentration. For the G461A variant, a sample of the flow-through (from TMC washing after lysate addition to the column) was also measured for activity and protein concentration.

For the G461A mutant, the fractions representing the active peak were pooled together. For the W460I mutant, the fractions were kept separated. Samples were stored at -20°C.

2.3.4 SDS polyacrylamide gel electrophoresis (SDS-PAGE)

The purified protein samples were analyzed with SDS-PAGE to determine their purity. SDS-PAGE was also performed on samples taken at different times during the purification process. Precasted NuPage™ 4-12% Bis-Tris gels with 1.0 mm wells (Thermo Fisher Scientific, USA) were used for the electrophoresis.

The samples were prepared by mixing 10 µl of enzyme sample with 5 µl buffer (NuPage™ LDS Sample buffer [4x]), 1 µl DTT and 4 µl H_2O. For reference, a ladder sample was prepared using the same materials applying 10 µl ladder instead of enzyme sample. The samples were mixed with centrifugation for few seconds and subjected to heat-shock (90°C for 2-3 minutes and immediately put on ice). Cooled samples were loaded to the wells of the gel and 1x NuPage® MES buffer (Thermo Fisher Scientific, USA) was added to the caseete. The cassette connected to a power source of 150 V until the lowest bands had reached the bottom of the gel (~ 60-90 minutes). The gel was stained with Coomassie-Blue R250 overnight and destained with a 30% (v/v) methanol solution for approx. 24 h. The destaining process was monitored at intervals and the methanol solution renewed.

2.4 Determination of protein concentration

Protein concentrations of purified enzyme samples were determined with Zaman and Verwilghen's method [26], a modified version of Bradford's method [27]. The method is based on the protein binding of Coomassie Brilliant Blue G-250 (CBBG).

A standard curve for the assay had previously been made with an 80 mg/ml protein standard (5 parts bovine serum albumin and 3 parts IgG), diluted to 0.4 mg/ml. The diluted standard was used to make up seven samples of 250 µl containing 10 – 100 µg of protein. Each sample was added to 2.75 ml of CBBG dye. The samples were done in triplicates. A blank, containing 250 µl H_2O and 2.75 ml CBBG dye, was used to calibrate the instrument. After a few minutes, absorbance was measured at 620 nm. According to the literature, the ideal period for measurements is between 5 and 20 minutes after combining sample and dye [27]. Figure 33 in Appendix B shows the standard curve.

The protein concentration of purified enzyme samples was measures, as well as the protein concentration of samples taken at different times during the purification process. The samples were diluted as needed to obtain an absorbance value that fit within the standard

curve. To prepare the samples, 100 µl of enzyme sample (diluted as needed) and 150 µl H_2O were added to 2.75 ml CBBG dye. The samples were done in triplicates. After a few minutes, the absorbance was measured at 620 nm. A blank was prepared as for the standard samples.

For rapid assessment of protein concentration of samples, absorbance at 280 nm was measured. Extinction coefficients of 61 310 $M^{-1}cm^{-1}$ and 55 935 $M^{-1}cm^{-1}$ were used for the G461A variant and W460I variant, respectively [14].

2.5 Enzyme kinetics

2.5.1 Standard activity analysis

Activity assays were performed at either 10°C or at room temperature on a Peltier temperature-regulated Evolution 220 spectrophotometer (Thermo Fisher). For assays performed at 10°C, the cuvettes were prechilled to prevent fog from forming on them during measurements. In general, each data point was measured in triplicates.

For *standard activity assays*, 10 µl enzyme solution was mixed with 990 µl reaction solution (5 mM *p*-nitrophenyl phosphate in DAE buffer [1.0 M diethanolamine, 1 mM $MgCl_2$, pH 9.8]). The hydrolysis of *p*-nitrophenyl phosphate (*p*NPP) to *p*-nitrophenol (*p*NP) was monitored at 405 nm for 30 seconds, at 25°C [28].

To determine kinetic parameters of mutants, assays were made with varying concentration of *p*NPP (0.0 – 2.5 mM for variant W460I and 0.0 – 5.0 mM for variant G461A). *p*NPP was dissolved in Caps buffer (100 mM Caps, 500 mM NaCl, 1.0 mM $MgCl_2$, pH 9.8) to a concentration of 5 mM and diluted with the same buffer to a desired concentration. Ten µl of enzyme solution were mixed with 990 µl reaction buffer and the hydrolysis of *p*NPP monitored at 405 nm for 30 seconds at 10°C. For exact substrate concentrations, the reaction buffer solutions, spiked with wild-type enzyme, were stored at room temperature overnight and the absorbance at 405 nm measured.

The enzyme activity (U/ml) was determined by the spectrometer's program using Beer's law and an extinction coefficient of 18.5 $mM^{-1}cm^{-1}$. GraphPad Prism® was used to fit results to appropriate derivations of the Michaelis-Menten equation and determine kinetic parameters.

2.5.2 Enzyme – inhibitor kinetic assay

Wild-type enzyme was used to determine the inhibitory effect of desthiobiotin (DDB) on VAP. To determine kinetic parameters, assays were made with varying concentration of *p*NPP, approx. 0.0 – 10 mM (exact range of concentrations varied between assays). *p*NPP was dissolved in Caps buffer (100 mM Caps, 1.0 mM $MgCl_2$, pH 9.8) to a concentration of 5 or 10 mM and diluted with the same buffer to a desired concentration. Three concentrations of DDB were analyzed – 2.5 mM, 0.25 mM and 0.05 mM. The effect of NaCl was also tested for 0.25 mM DDB. For control, assays were made without DDB.

Ten µl of enzyme solution were mixed with 990 µl reaction solution and the hydrolysis of *p*NPP monitored at 405 nm for 30 seconds at 10°C. The enzyme activity (U/ml) was determined by the spectrometer's program using Beer's law and an extinction coefficient of 18.5 $mM^{-1}cm^{-1}$. GraphPad Prism® was used to fit results to appropriate derivations of the Michaelis-Menten equation and determine kinetic parameters. For exact substrate concentrations, the reaction solutions, spiked with wild-type enzyme, were stored at room temperature overnight and the absorbance at 405 nm measured.

2.6 Stability measurements

Circular dichroism (CD) spectroscopy was used to determine global temperature stability of mutants. Mutants' resistance to urea was determined with kinetic analysis and fluorescence measurements. The dimer-monomer equilibrium was also assessed for the G461A variant.

2.6.1 Urea denaturation and inactivation

The mutants were subjected to various urea concentrations, ranging from 0.0 to 5.0 M. Urea was added to Mops buffer (25 mM Mops, 1 mM $MgSO_4$, pH 8.0) to a final volume of 450 µl. 50 µl of enzyme solution were added to the samples for a final protein concentration of 0.07 mg/ml and 0.02 mg/ml for variant W460I and G461A, respectively. The samples were incubated at 10°C overnight.

Fluorescence measurements were performed on the samples before their activity was determined with the standard activity assay described in section 2.5.1.

2.6.2 Fluorescence spectroscopy

Fluorescence spectroscopy was used to study the enzymes quaternary structure dissociation. Emission spectra were recorded from 310 to 400 nm with 0.5 nm increments, using a fixed excitation wavelength of 295 nm. The spectra were recorded at 10°C on a FluoroMax4 (Horiba). To eliminate noise from the spectra, three blanks were made with urea concentration of 0.0 M, 2.0 M and 5.0 M. The emission of the 0.0 M blank was subtracted from the emission of the other two blanks. The average emission of the subtracted 2.0 M and 5.0 M blanks' spectra was used to make a spectrum for 3.5 M urea blank. That spectrum was then multiplied with the appropriate coefficient to a desired urea concentration and subtracted from the samples' spectra. The emission of the 0.0 M blank was also subtracted from the samples' spectra.

The spectra were fitted to a 3rd degree polynomial in the range between 330 and 370 nm. λ_{max} was calculated for each of the spectra. The shift in emission spectrum with increased urea concentration was also monitored by comparing the ratio of emission at two wavelengths (355:348 nm) at either side of λ_{max}.

2.6.3 CD spectroscopy

Global temperature stability of the mutants was determined with CD spectroscopy. The measurements were carried out in Mops buffer (25 mM Mops, 1 mM $MgSO_4$, pH 8.0). Because enzymes were stored in a TMC buffer, the sample had to be dialyzed. A dialysis tubing made of cellulose was washed in water. Approx. 1 ml of enzyme solution was added to the tube and the ends closed with clips. The sample was placed in a beaker containing 1 L of the Mops buffer. The dialysis was carried out at 4°C with gentle stirring overnight.

Before CD was measured, the samples were diluted to an appropriate concentration (approx. 6 μM, measured by absorbance at 280 nm). CD was measured in a Jasco J-1100 CD spectrometer and temperature was controlled with a Jasco CTU-1100 circulating thermostat unit. Measurements were done using either a 2 mm cuvette (variant W460I) or a 1 mm cuvette (variant G461A).

First, the spectrum was measured from 200-250 nm at 25°C in triplicate, and an appropriate wavelength chosen for temperature stability measurements. Change in CD signal was monitored at 222 nm, from 20°C to 90°C. The temperature increase rate was 1°C/min. The measurements were done in triplicates.

2.6.4 Dimer-monomer equilibrium

To study the dimer-monomer equilibrium, enzyme dilution assays were performed, starting with different concentrations. The equilibrium was only assessed for the G461A variant. The activity of the W460I variant was insufficient for measurements at such low enzyme concentration.

A total of four assays were performed. For every assay, enzyme was added to 10 ml appropriate buffer to obtain a final concentration of either 10 mM, 25 mM or 50 mM dimer concentration. The resultant enzyme solutions were used as the first samples of the series (sample 1). For the first three series, the dilution was completed in the following manner, to give a total of 12 samples for each series: 3.5 ml buffer was added to a test tube. 6.5 ml of enzyme solution from sample 1 were transferred to test tube 2 and mixed well (by pipetting up and down a few times or by closing the tube with parafilm and inverting it). 6.5 ml of solution from sample 2 were then transformed to test tube 3 etc. The forth series was diluted in the same manner except 4 ml of buffer were added to each test tube and 4 ml of enzyme solution were transferred between them. The samples were incubated overnight, either at 10°C or 25°C, before their activity was measured.

The first assay was composed of two mutant enzyme dilution series. The series were made with TMC buffer (20 mM Tris, 10 mM $MgCl_2$, pH 8.0). NaCl was added to one series to a final concentration of 500 mM (series 1a). The other series (1b) had no salt added. Enzyme was added to 10 ml of the appropriate buffer from a 39 μM stock to obtain 50 nM dimer concentration and then diluted as described above. The enzyme samples were incubated overnight at 10°C. Activity was measured at pH 8.0 and 25°C.

Ten µl of reaction solution (50 mM *p*NPP dissolved in TMC buffer) were mixed with 990 µl enzyme solution. Activity of samples was measured at 450 nm and 405 nm for series 1a and 1b, respectively. Each series was done in duplicates and each data point was generally measured in duplicates (Table 2.3).

Table 2.3. Buffers and conditions of the first dilution assay.

Series	Buffer	Incubation temperature	Activity measurement conditions
1a – With NaCl	20 mM Tris 10 mM $MgCl_2$ 500 mM NaCl pH 8.0	10°C	25°C pH 8.0 450 nm
1b – Without NaCl	20 mM Tris 10 mM $MgCl_2$ pH 8.0	10°C	25°C pH 8.0 405 nm

The second assay consisted of three mutant enzyme dilution series. All three series were made with 50 mM Tris buffer (50 mM Tris, pH 8.0). NaCl was added to one series to a final concentration of 500 mM (series 2a). $MgCl_2$ was added to a second series to a final concentration of 10 mM (series 2b). For reference, the third series had no salt added (series 2c). Enzyme was added to 10 ml of the appropriate buffer from a 39 µM stock to obtain 10 nM dimer concentration and diluted as described above. The enzyme samples were incubated overnight at 10°C. Activity was measured at pH 8.0 and 10°C.

Ten µl of reaction solution (50 mM *p*NPP in the respective buffer) were mixed with 990 µl enzyme solution and the activity measured at 405 nm. Each datapoint was generally measured in triplicates (Table 2.4).

Table 2.4. Buffers and conditions of the second dilution assay.

Series	Buffer	Incubation temperature	Activity measurement conditions
2a – With NaCl	50 mM Tris 500 mM NaCl pH 8.0	10°C	10°C pH 8.0 405 nm
2b – With $MgCl_2$	50 mM Tris 10 mM $MgCl_2$ pH 8.0	10°C	10°C pH 8.0 405 nm
2c – Without salt	50 mM Tris pH 8.0	10°C	10°C pH 8.0 405 nm

The third assay was composed of four wild-type enzyme dilution series. The series were made with 50 mM Tris buffer (50 mM Tris, pH 8.0). NaCl was added to two series to a final concentration of 500 mM (series 3a and 3c). The other series (3b and 3c) had no salt added. Enzyme was added to 10 ml of the appropriate buffer from a 86.5 µM stock to obtain 25 nM dimer concentration and then diluted as described above. The enzyme samples were incubated overnight at either 10°C (series 3a and 3b) or 25°C (series 3c and 3d). Activity of series 3a was measured at 10°C and pH 8.0 at 450 nm. Activity of series 3b was measured

at 10°C and pH 8.0 at 405 nm. Activity of series 3c and 3d was measured at 25°C and pH 8.0 at 405 nm.

Fifty µl reaction solution (50 mM *p*NPP in the respective buffer) were mixed with 950 µl enzyme solution. Each datapoint was generally measured in triplicates (Table 2.5).

Table 2.5. Buffers and conditions of the third dilution assay.

Series	Buffer	Incubation temperature	Activity measurement conditions
3a – NaCl, 10°C	50 mM Tris 500 mM NaCl pH 8.0	10°C	10°C pH 8.0 450 nm
3b – No salt, 10°C	50 mM Tris pH 8.0	10°C	10°C pH 8.0 405 nm
3c – NaCl, 25°C	50 mM Tris 500 mM NaCl pH 8.0	25°C	25°C pH 8.0 405 nm
3d – No salt, 25°C	50 mM Tris pH 8.0	25°C	25°C pH 8.0 405 nm

The fourth assay was composed of two mutant and two wild-type enzyme dilution series. The series were made with 50 mM Caps buffer (50 mM Caps, pH 9.8). Enzyme was added to 10 ml of the appropriate buffer from an enzyme stock solution (39 µM and 86.5 µM of mutant and wild-type, respectively) to obtain 10 nM dimer concentration and then diluted as described above. The enzyme samples were incubated overnight at either 10°C (series 4a and 4c) or 25°C (series 4b and 4d). Activity of all series was measured at 25°C and pH 9.8 at 405 nm.

50 µl reaction solution (50 mM *p*NPP in the respective buffer) were mixed with 950 µl enzyme solution. Each datapoint was generally measured in triplicates(Table 2.6).

Table 2.6. Buffers and conditions of the fourth dilution assay.

Series	Buffer	Incubation temperature	Activity measurement conditions
4a – Mutant	50 mM Caps pH 9.8	10°C	10°C pH 9.8 450 nm
4b – Mutant	50 mM Caps pH 9.8	25°C	25°C pH 9.8 405 nm
4c – Wild-type	50 mM Caps pH 9.8	10°C	10°C pH 9.8 405 nm
4d – Wild-type	50 mM Caps pH 9.8	25°C	25°C pH 9.8 405 nm

3 Results

3.1 Preparation of mutated plasmids

3.1.1 Plasmid preparation

Desired mutations were introduced into *p*ET11a plasmid vector using QuikChange® site-directed mutagenesis. A total of five mutated plasmid strains were prepared – W460I, G461A, G461S, T462A and T462S. The amino acids chosen for mutation are all situated in the dimer's surface loop and well conserved.

The amount of dsDNA template needed for QuikChange® site-directed mutagenesis can vary but should be between 5 and 50 ng. To determine the appropriate amount of the dsDNA template for this study, two samples were made for the mutagenesis of variant W460I, one with 20 ng dsDNA template and one with 50 ng. Figure 12 shows the agar plates for each sample. It was obvious that 20 ng of the dsDNA template was not enough, and it was decided to use 50 ng of template for the other four variants.

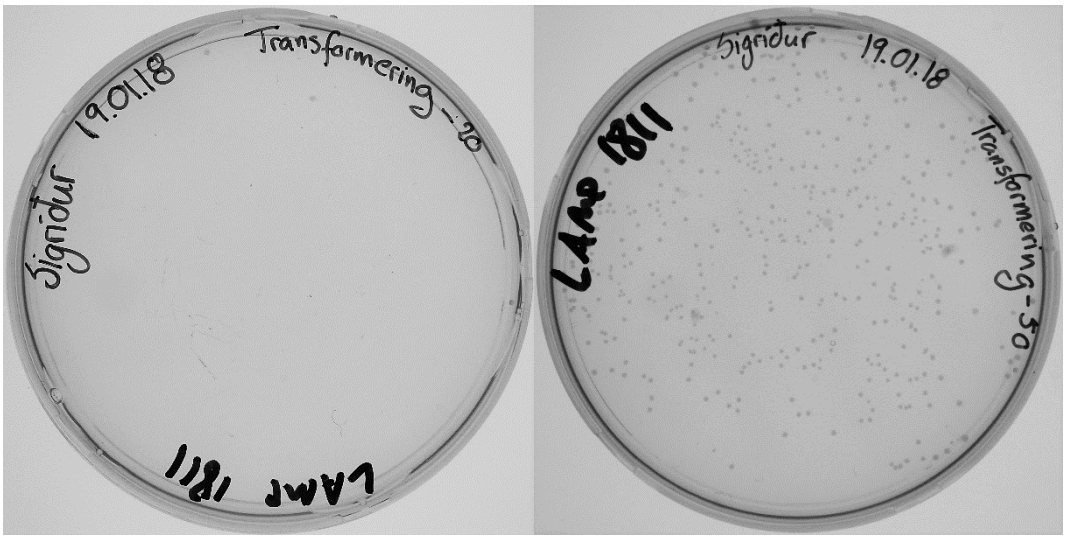

Figure 12. The agar plate cultures for W460I mutated cultures.
Mutated pET11a plasmids were transformed into E. coli XL10-Gold ultracompetent cells. The cells were incubated on LB agar plates containing ampicillin (100 µg/ml) at 37°C overnight. ***a.*** *20 ng dsDNA template were used for the mutagenesis. Hardly any colonies grew on the agar overnight.* ***b.*** *50 ng dsDNA template was used for the mutagenesis. An adequate number of colonies grew on the agar overnight.*

3.1.2 Plasmid purification

For each variant, 3 colonies were cultured 5 ml LB medium containing ampicillin (100 µg/ml) at 37°C overnight. Subsequently, the plasmids were isolated and purified with GeneJET™ Plasmid Miniprep Kit. To confirm the purity of the samples and the integrity of the plasmids, the samples were subjected to agarose gel electrophoresis (Figure 13). Plasmid samples were also sent for sequencing to confirm the presence of the mutation. Results from the DNA sequencing, for the strains used in this study, can be seen in Appendix B.

Electrophoresis of trains G46a1S-2 and T461A-1 (wells **b**6 and **c**1, respectively) did not show a band for the VAP gene. All other plasmid samples were deemed pure by the results from the electrophoresis. DNA sequencing confirmed successful mutation for at least one strain of each mutated plasmid. Two strains were chosen for further studies – W460I-3 (well **a**4) and G461A-2 (well **b**3).

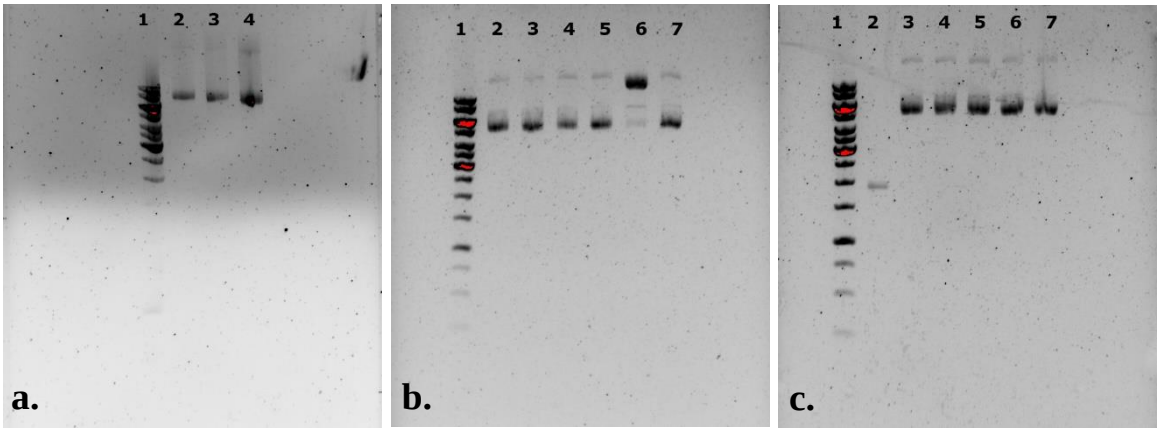

Figure 13. Gel electrophoresis of purified mutated plasmids.
*Purified plasmids were subjected to electrophoresis for confirmation of purity and integrity of the plasmids. Wells **a**4 and **b**3 contain the strains used for this study (W460I-3 and G461A-2, respectively). For all images, well 1 contains the ladder **a.** W460I variant, wells 2-4 contain strains 1-3, respectively. **b.** Wells 2-4 contain variant G461A (strains 1-3, respectively). Wells 5-7 contains G461S variant (strains 1-3, respectively). **c.** Wells 2-4 contain variant T462A (strains 1-3, respectively). Wells 5-7 contain variant T462S (strains 1-3, respectively).*

3.2 Enzyme expression and purification

3.2.1 Enzyme purification – variant G461A

Figure 14 shows results from activity measurements of selected fractions of purified enzyme. Activity was measured as standard activity under transphosphorylating conditions (see section 2.5.1). Fraction 32 had the highest observed activity of 28 486 U/ml.

Fractions 23 – 50 were pooled together. The activity of the pooled sample was 11 925 U/ml. The sample was divided into 1 ml portions and snap-frozen in liquid N_2.

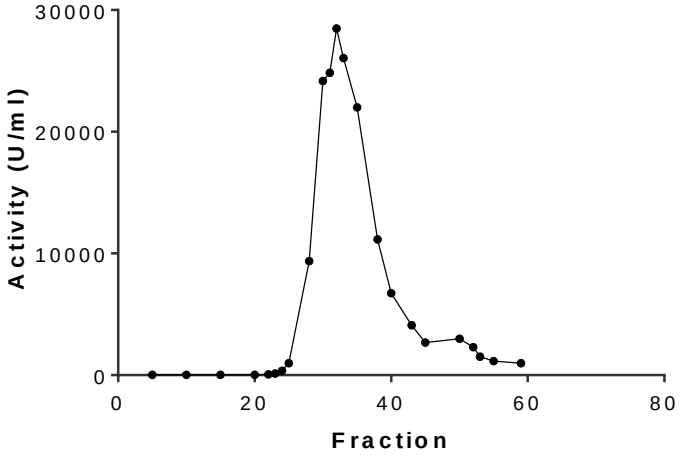

Figure 14. Activity of collected fractions of purified G461A.
The enzyme was purified on a Strep-*Tactin® affinity column. The enzyme was washed of the column with desthiobiotin and collected into Eppendorf tubes in 1 ml fractions. Standard activity of selected elution fractions was measured under transphosphorylating conditions in DEA buffer at pH 8.0 and 10°C. Only the elution is shown here.*

Table 3.1 summarizes the protein purification process. Standard activity and protein concentration were measured for purified enzyme, lysate, flow-through and NaCl eluate. Protein concentration was determined with Zaman and Verwilghen's method (see method description in section 2.4). The purification process gave 15 ml of purified enzyme sample or 32.8 mg protein. The purified enzyme's specific activity was determined to be 6150 U/mg.

Table 3.1. Summary of the purification process of VAP mutant G461A.
Activity was measured with 5 mM p*NPP under transphosphorylating conditions in DAE buffer at pH 8.0 and 10°C. Protein concentration was determined with Zaman and Verwilghen's method. The enzyme was purified with* Strep-*Tactin® affinity column.*

Sample	Volume (ml)	Activity (U/ml)	Protein conc. (mg/ml)	Enzyme units (U)	Total protein (mg)	Specific activity (U/mg)	Yield (%)	Purification (fold)
Lysate	106	3648	9.15	386 688	970	399	100	1.0
Flow-through	100	12.0	9.60	1200	960	1.3	31	0.0
NaCl eluate	27.0	0.33	0.24	9.00	6.5	1.4	0	0.0
Purified	15.0	11 930	1.94	179 000	32.8	6150	46	15.4

The samples were subjected to SDS-PAGE electrophoresis to determine their purity and monitor the purification process. Figure 15 shows the results from SDS-PAGE run of samples from the purification of both the G461A and W460I variant.

As could be expected, the lysate and flow-through samples contained an abundance of proteins and it is not possible to distinguish any individual bands (lanes 2 and 3, respectively). The NaCl eluate also contained many different proteins (lane 4). A band can be detected where the VAP enzyme is expected, around 56 kDa, indicating that some of the enzyme got lost when the column was washed with the TMC + NaCl buffer. For the purified enzyme sample, a strong band is detected at 63.2 kDa (lane 5). That is a little bit higher than the 55 kDa expected. As evident by the inclining lanes, the gel got probably too hot. This skews the ladder bands' positions relative to the sample bands and makes size determination less reliable.

The results of the W460I samples will be discussed in the next section.

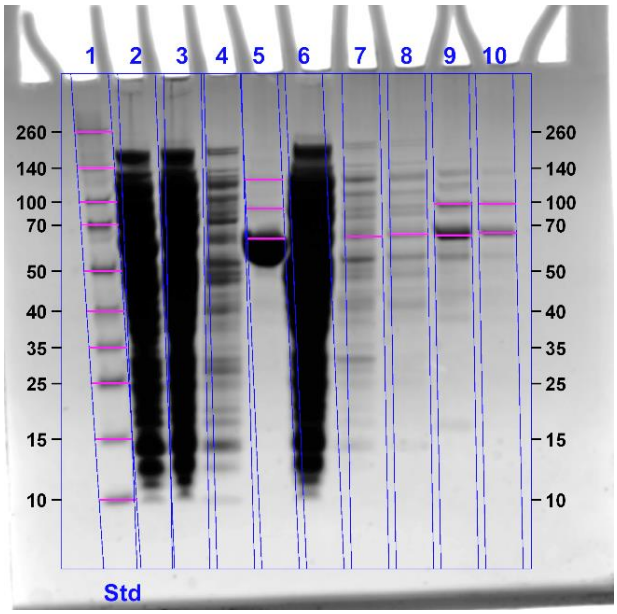

Figure 15. Results from SDS-PAGE run of purified variants G461A and W460I, and of samples taken at different points of the purification process
Lane 1: Ladder. Lane 2-5: ***Variant G461A****, Lysate, Flow-through, NaCl eluate, Purified enzyme (respectively) Lane 6-10:* ***Variant W460I****, Lysate, NaCl eluate, Purified enzyme (Left tail, middle and Right tail of the activity peak) (respectively).*

3.2.2 Enzyme purification – variant W460I

Figure 16 shows results from activity and protein concentration measurements of elution fractions. The two peaks aligned well together. Fraction 35 had the highest activity measured (2.674 U/ml) and fraction 36 had the highest protein concentration measured (33 µg/ml).

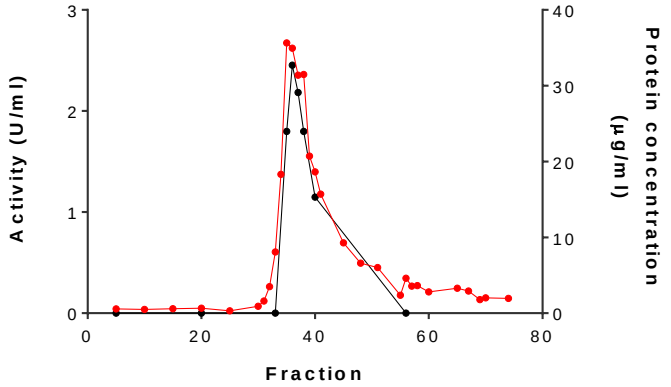

Figure 16. Activity and protein concentration of collected fractions from elution of variant W460I.

The enzyme was purified with Strep-*Tactin® affinity column. The enzyme was washed off the column with d-Desthiobiotin and collected into Eppendorf tubes in 1 ml fractions.* ***Red:*** *Standard activity of selected fractions was measured under transphosphorylating conditions in DEA buffer at pH 8.0 and 10°C.* ***Black:*** *Protein concentration of selected fractions was determined with Zaman and Verwilghen's method.*

Table 3.2 summarizes the protein purification process. Standard activity and protein concentration was measured for purified enzyme, lysate and NaCl eluate. Protein concentration of lysate and NaCl eluate was determined with Zaman and Verwilghen's method (see method description in section 2.4). Protein concentration of purified enzyme is the average concentration of fractions 34 – 40 (the fractions constituting the active peak) as measured by absorbance at 280 nm. The results from the purification of variant W460I look rather odd and will be discussed further in section 4.1.

Table 3.2. Summary of the purification process of VAP mutant G461A.

Activity was measured with 5 mM p*NPP under transphosphorylating conditions in DAE buffer at pH 8.0 and 10°C. Protein concentration was determined with Zaman and Verwilghen's method. Values for purified sample were calculated as the mean activity and protein concentration of seven 1 ml fractions. The enzyme was purified with* Strep-*Tactin® affinity column.*

Sample	Volume (ml)	Activity (U/ml)	Protein conc. (mg/ml)	Enzyme units (U)	Total protein (mg)	Specific activity (U/mg)	Yield (%)	Purification (fold)
Lysate	100	0.49	13.2	49.2	1320	0.04	100	1.0
NaCl eluate	22.5	0.05	0.3	1.1	6.3	0.17	2	4.7
Purified	7	2.05	0.001	18.4	0.01	1590	37	42 600

The samples were subjected to SDS-PAGE electrophoresis to determine their purity and monitor the purification process. Figure 15 (section 3.2.1) shows the results from SDS-PAGE run of samples from the purification of both the G461A and W460I variant. As for the G461A variant, the W460I lysate contained an abundance of proteins and no bands could be distinguishe (lane 6). The NaCl eluate also contained many proteins and a possible VAP band can be detected (lane 7). Three fractions of the purified enzyme were subjected to electrophoresis, fractions F5, F39 and F52 (lanes 8, 9 and 10, respectively). F5 is a part of the tail before the activity and protein concentration peak, F52 is a part of the tail after the peak and F39 is close to the top of the peak. Of the three fractions, F5 had the most impurities. Most likely they were lingering impurities after the NaCl elution of the column. A VAP band can be detected in the sample indicating that some enzyme was lost in the fractions, not counted as a part of the peak. For the F39 sample, a strong VAP band was detected at 64.9 kDa, although much fainter than the one in the G461A purified enzyme sample. Generally, a thicker band indicates higher enzyme concentration. The F39 sample also contained some impurites that could possibly have affected the results. Not surprisingly, the F52 sample contained some VAP enzyme. It also contained the least amount of impurities of all three fraction samples.

3.3 Enzyme kinetics

The mutants' kinetic parameters were determined as described in section 2.5.1. Akaike's Information Criteria (AICc) was used to select which model the data was fitted to, the Michaelis-Menten equation or the substrate-inhibition equation. AICc compares the fit of two models to a certain data set and tells how much more likely on model is to be the correct one compared to the other model. For the G461A variant, the substrate-inhibition model was 15 times more likely than the Michaelis-Menten model to be correct. Therefore, the data was fitted to the substrate-inhibition equation. The data for variant W460I was fitted to the Michaelis-Menten equation. However, the AICc results were not as conclusive as for variant G461A and the Michaelis-Menten model was only 3.6 times more likely than the substrate-inhibition model to be correct. Figure 17 shows the activity measured for G461A and W460I variants with the data fitted to substrate-inhibition and Michaelis-Menten equation, respectively.

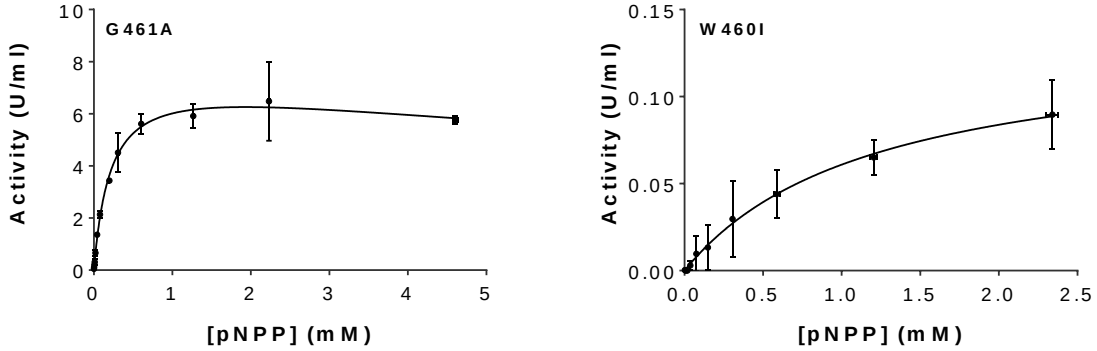

Figure 17. Enzyme activity curves of mutants G461A and W460I.
Activity of purified mutants was measured under nontransphosphorylating conditions in Caps buffer at pH 9.8 and 10°C. GraphPad Prism® was used to fit the curves and calculate kinetic parameters. Mutant G461A was fitted to a substrate-inhibition equation. Mutant W460I was fitted to the Michaelis-Menten equation. Kinetic parameters are shown in Table 3.3.

Kinetic parameters for G461A and W460I variants are summarized in Table 3.3. K_m and K_i values were obtained using GraphPad Prism®. The program was also used to determine V_{max} for k_{cat} values which were calculated by dividing V_{max} with enzyme concentration. Michaelis-Menten kinetic parameters (MM-fit) for wild-type VAP were obtained from a previous study [14]. This study is the first to determine kinetic parameters from fitting activity measurements to a substrate-inhibition equation (SI-fit). The parameters were calculated for the enzyme-inhibitor assay (see section 3.7.1). Measurements were performed under the same conditions as the current enzyme kinetic measurements.

The W460I mutation resulted in almost complete loss of activity. K_m of the variant was 6-fold higher than wild-type VAP – 1.21 mM and 0.19 mM, respectively. The k_{cat} value of the mutant was less than 0.25% of the wild-types k_{cat} value – 0.70 s^{-1} and 302 s^{-1}, respectively. The mutant had lost more than 99.9% of its catalytic efficiency, described as k_{cat}/K_m. The mutant's catalytic efficiency was 0.58 $s^{-1}mM^{-1}$ compared to 1560 $s^{-1}mM^{-2}$ for the wild type. This low activity of the mutant made activity measurements difficult and resulted in high standard deviations. It is also possible that the measured activity was that of the impurities in the sample (Figure 15).

When fitted to the Michaelis-Menten equation (MM-fit) the G461A mutation did not seem to have any effect on the enzymes activity. However, there might be some difference in kinetic parameters determined with fitting the data to a substrate-inhibition equation (SI). It is possible that the mutant's K_m value is increased to 0.22 mM from the wild-types K_m value of 0.14 mM. The results indicate also a possible decrease in k_{cat} and k_{cat}/K_m due to the mutation. The mutant had k_{cat} and k_{cat}/K_m values of 327 s^{-1} and 1520 $s^{-1}mM^{-1}$,

respectively, while the wild-type had k_{cat} and k_{cat}/K_m values of 415 s^{-1} and 3050 $s^{-1}mM^{-1}$, respectively. However, the results show relatively high standard deviations which makes comparison difficult.

Table 3.3. Kinetic parameters of variants G461A and W460I, compared to wild-type VAP. *Kinetic activity of mutants was measured at various substrate concentrations. The data were fitted to a nonlinear regression with GraphPad Prism®, either to the Michaelis-Menten equation (MM) or to a substrate-inhibition equation (SI). Substrate-inhibition parameters for wild-type VAP were calculated in the desthiobiotin inhibition study (section 3.7). Michaelis-Menten kinetic parameters (MM-fit) for wild-type VAP were obtained from a previous study* [14] *K_i describes the dissociation constant for binding of two substrate molecules to the enzyme. Values are given with standard error.*

Mutant	Fit	K_m (mM)	k_{cat} (s^{-1})	k_{cat}/K_m ($s^{-1}mM^{-1}$)	K_i (mM)
W460I	MM	1.21 (0.34)	0.70 (0.23)	0.579 (0.355)	n/a
G461A	MM	0.16 (0.02)	281 (34)	1810 (440)	n/a
Wild-type	MM	0.19 (0.03)	302 (20)	1560 (260)	n/a
G461A	SI	0.22 (0.04)	327 (53)	1520 (493)	17.3 (7.4)
Wild-type	SI	0.14 (0.04)	415 (50)	3050 (1309)	6.0 (2.2)

3.4 Effect of urea on activity and structural stability

3.4.1 Structural stability of G461A mutant in urea

Samples were prepared according to Table B.1 (see Appendix B) and incubated at 10°C overnight. The samples fluorescence was then analyzed (see section 2.6.2). The emission spectra can be seen in Figure 18. The lighter colored lines represent the lower urea concentration levels and the darker lines represent the higher urea concentration levels. In general, the spectra of the enzymes incubated at higher urea concentration exhibited a red shift with respect to the spectra of the enzymes incubated at lower urea concentration levels. This shift was confirmed with a red shift of λ_{max}, from 340 nm to 358 nm (Figure 19a). The ratio of emission intensity at two wavelengths – 355 nm and 348 nm – was also assessed (Figure 19b). At lower urea concentrations, the emission intensity was higher at 348 nm than at 355 nm. As urea concentration increased, the emission intensity at 355 nm increased compared to that at 348 nm. This fact would also indicate a red shift of the spectra.

The shift in spectra indicates a change in the environment of tryptophan residues and thus, a change in the enzyme's quaternary structure. The curve in Figure 19a, indicating the change in λ_{max}, has a sigmoidal shape, with plateaus below 0.5 M urea and above 2.6 M urea. The curve in Figure 19b, indicating the change in emission ratio, also shows a plateau above 2.6 M, but does not have a clear plateau at lower urea concentrations.

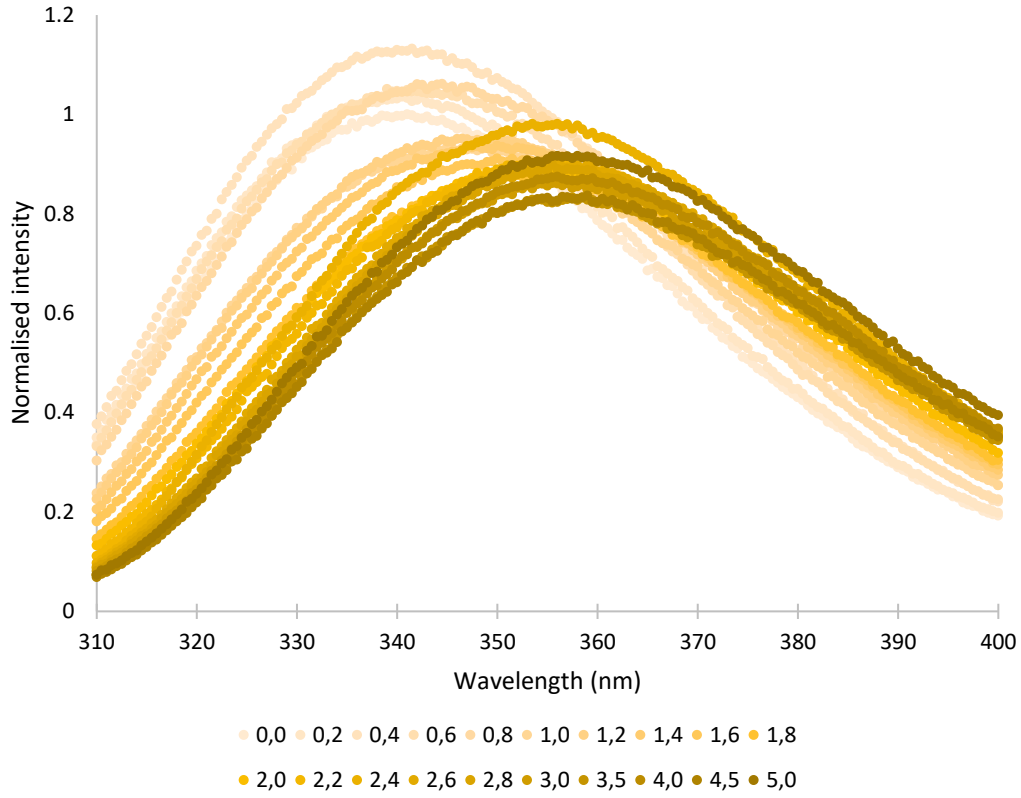

Figure 18 Emission spectra of the G461A mutant after incubation in urea.
Enzyme samples were incubated in various urea concentrations overnight at 10°C. Fluorescence spectroscopy was used to monitor changes in the enzymes structure. The spectra exhibited a red shift for samples incubated at higher urea concentrations, from 340 nm to 358 nm. This shift indicates a change in the environment of tryptophan residues and thus, a change in the enzymes quaternary structure.

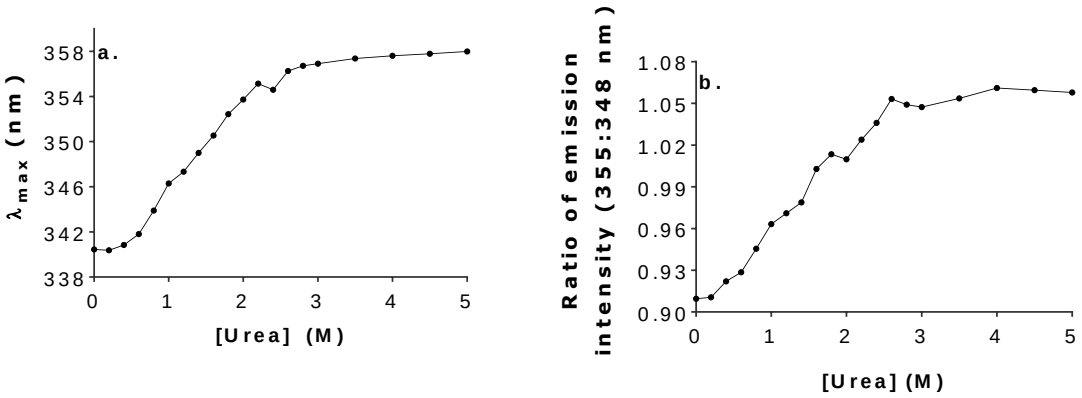

Figure 19. A change in λ_{max} in the emission spectrum of mutant G461A.
a. *λ_{max} is shifted from 340 nm to 358 nm with increased urea concentration.* ***b.*** *The ratio of emission intensity at two wavelengths changes with increased urea concentration. Both figures indicate a red shift of the spectra.*

3.4.2 Structural stability of W460I mutant in urea

Samples were prepared according to Table B.1 (see Appendix B) and incubated at 10°C overnight. The samples fluorescence was then analyzed as described in section 2.6.2. The emission spectra can be seen in Figure 20. The lighter colored lines represent the lower urea concentration levels and the darker lines represent the higher urea concentration levels.

The spectra for the W460I mutant showed similar patterns as the spectra for the G461A mutant. The spectra showed a right shift with increased urea concentration, confirmed with a shift in λ_{max} towards higher wavelengths (Figure 21a) and an increase in emission intensity at 355 nm compared to that at 348 nm (Figure 21b). However, the curve in Figure 21a, indicating change in λ_{max}, does not have a distinctive sigmoidal curve. It has a plateau at urea concentrations above 3.0 M but only a very vague plateau at low urea concentration levels.

In addition, the change in λ_{max} is less for the W460I mutant than for the G461A mutant. The W460I mutant's λ_{max} curve reaches its plateau at 354 nm compared to 358 nm for the G461A mutant. The curve in Figure 21b, indicating the change in emission ratio, is not as "clean" as the curve in Figure 19b but does seem to reach a plateau above 3.0 M urea concentration. Again, the change in ratio is less for the W460I mutant than for the G461A mutant in accordance with less shift in λ_{max}.

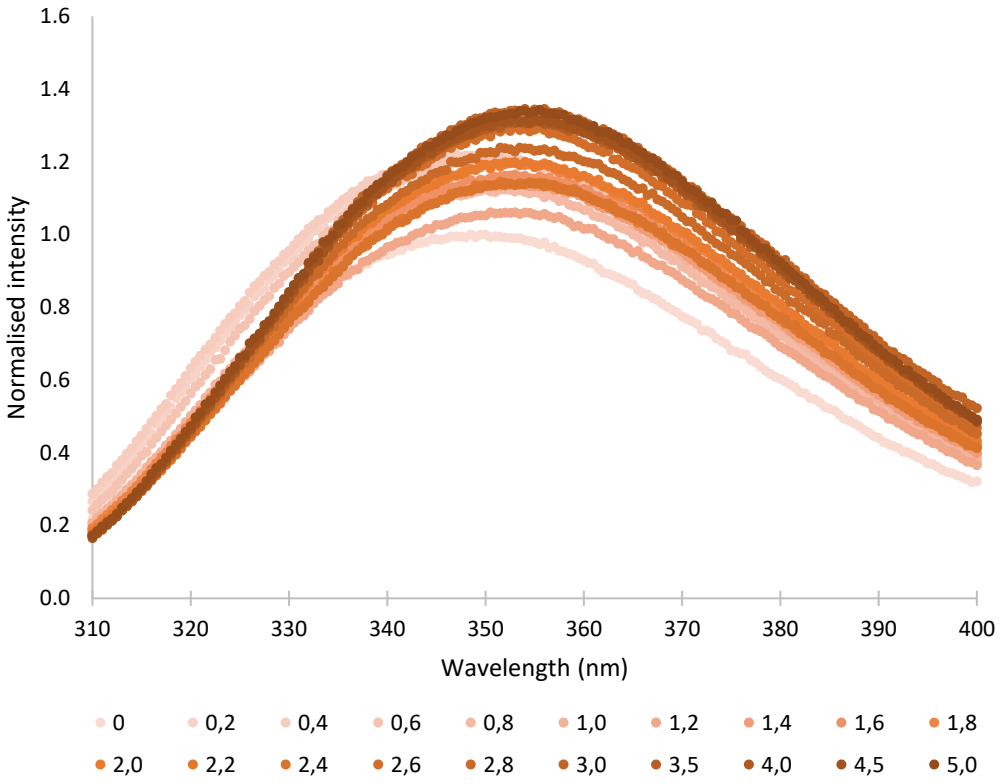

Figure 20. Emission spectra of the G461A mutant after incubation in urea.
Enzyme samples were incubated in various urea concentrations overnight at 10°C. Fluorescence spectroscopy was used to monitor changes the enzymes structure. The spectra exhibited a red shift for samples incubated at higher urea concentrations, from 349 nm to 355 nm. This shift indicates a change in the enzyme's quaternary structure.

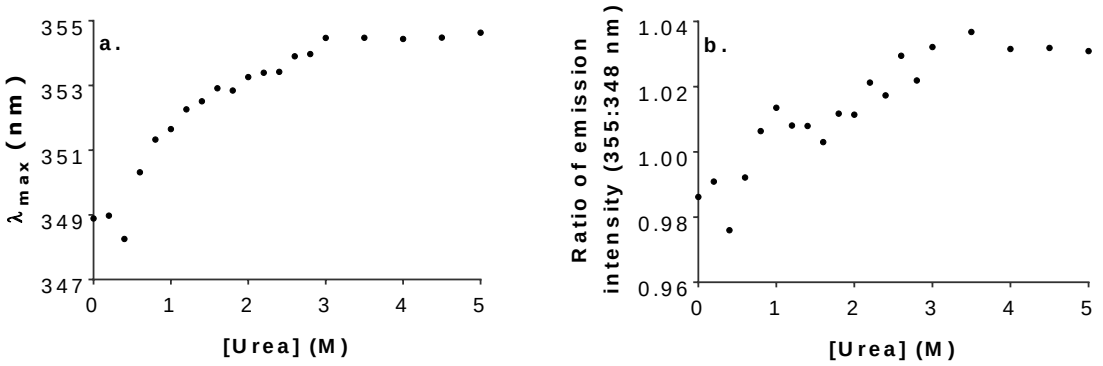

Figure 21. A change in λ_{max} in the emission spectrum of mutant W460I.
a. *λ_{max} is shifted from 349 nm to 355 nm with increased urea concentration.* ***b.*** *The ratio of emission intensity at two wavelengths changes with increased urea concentration. Both figures indicate a red shift of the spectra.*

3.4.3 Effect of urea on enzyme activity

The enzyme activity of the samples from the fluorescence spectroscopy analysis was measured as described in section 2.6.2. For both mutants, the activity decreases with increased urea concentration. For the G641A mutant, the activity was completely lost at urea concentrations above 2.0 M, little before the λ_{max} and emission-ratio curves reached plateaus. The W460I mutant, seemed to endure higher concentrations and its activity only starts to decrease at urea levels above 2.0 M (Figure 22a).

The absolute activity of the W460I mutant was much lower than that of the G461A mutant (Figure 22b). When the absolute activity was considered, the activity of the G461A mutant drops down to 0.047 (0.010) U/ml at 2.0 M urea whereas the W460I mutant still had an activity of 0.322 (0.018) U/ml at the same urea concentration. The W460I mutant had to be incubated in 4.0 M urea before its absolute activity droped below 0.05 U/ml (see Appendix B). The fluctuations and high standard deviations in activity measured for the W460I mutant are probably due to the low absolute activity and the difficulties in measuring such low activity.

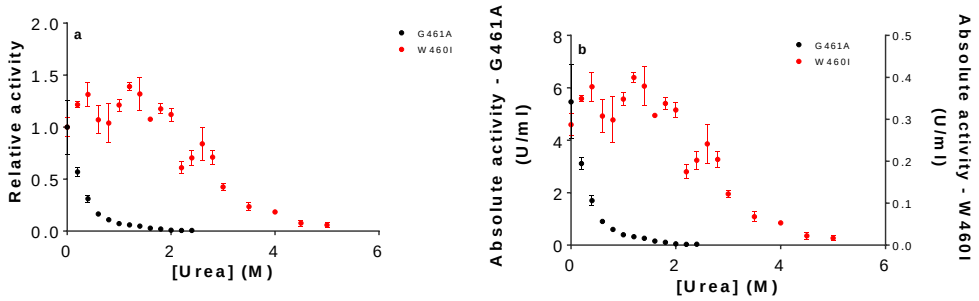

Figure 22. Effect of urea on G461A and W460I mutants.
The figures show ***a.*** *relative activity and* ***b.*** *absolute activity of variants G461A and W460I after incubation at various urea concentrations. For both enzymes, activity decreases with increased urea concentration. Variant W460I had much lower absolute activity than variant G461A, but it seemed withstand higher urea concentrations.*

3.5 Effect of temperature on structural stability

Global temperature stability of the mutants was determined with CD spectroscopy. The method is described in detail in section 2.6.3. The stability of three samples of each mutant were measured and melting temperature was determined for each sample. Melting temperatures of the mutants are reported as mean of the three samples (Table 3.4).

The inactivation and unfolding model of VAP has previously been shown to involve an inactive dimer and an inactive, unfolded monomeric state before the monomers unfold [14]. Therefore, the data was fitted with CDpal© (a CD spectrometry analysis program) to

a three state T_m function to determine two different melting temperatures of each sample (work performed by Jens G. Hjörleifsson).

Table 3.4. Melting points of variants G461A and W460I.
Melting temperatures of each variant were determined from CD spectroscopy results of three samples each. The circular dichroism was measured at 222 nm with a temperature increase of 1°C/min in the range of 20-90°C. Measurements were performed in Mops buffer (25 mM Mops, 1 mM $MgSO_4$, pH 8.0). Data was fitted to a three state T_m function to determine the melting points. Values are shown as a mean of three samples with standard error.

	G461A	**W460I**
T_m1 [°C]	44.5 (1.3)	46.3 (4.4)
T_m2 [°C]	53.1 (0.5)	68.1 (1.8)

The CD signal of the mutants was monitored at 25°C for a range of wavelengths, from 190 nm to 250 nm (Figure 23). The samples exhibited the strongest CD signal around 220 nm. Subsequently, a wavelength of 222 nm was chosen to monitor the thermal denaturation of the mutants.

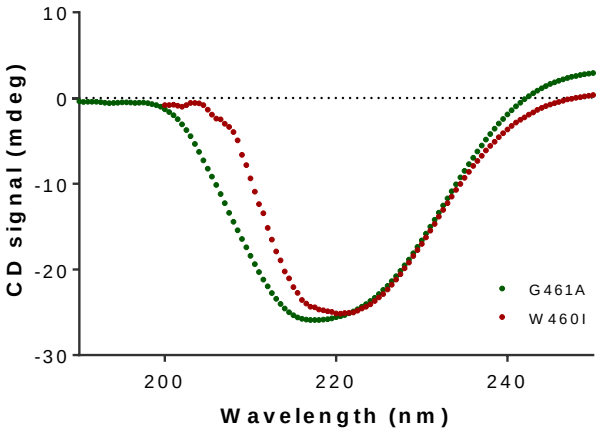

Figure 23. CD spectra of variants G461A and W460I.
The CD signal of the variants was monitored at wavelengths 190-250 nm. The wavelength corresponding to the strongest CD signal (222 nm) was chosen to monitor thermal denaturation of the mutants. The measurements were performed in Mops buffer (25 mM Mops, 1 mM $MgSO_4$, pH 8.0) at 25°C.

Figure 24 shows results for samples G46A-1 and W460I-1. The melting curve of the G461A mutant was as expected and shows obvious asymmetry, due to an intermediate state. The

intermediate plateau is not very distinctive, and it proved difficult to fit the data. This resulted in a rather high error of estimated values.

The melting curve of mutant W460I also shows an intermediate plateau. However, the curve is not as expected. CD signal at the highest temperatures is still relatively high, as if not all of the protein has unfolded. It is likely that the impurities in the sample (see section 3.2.2) are affecting the results, causing melting temperatures to be estimated higher than they really are.

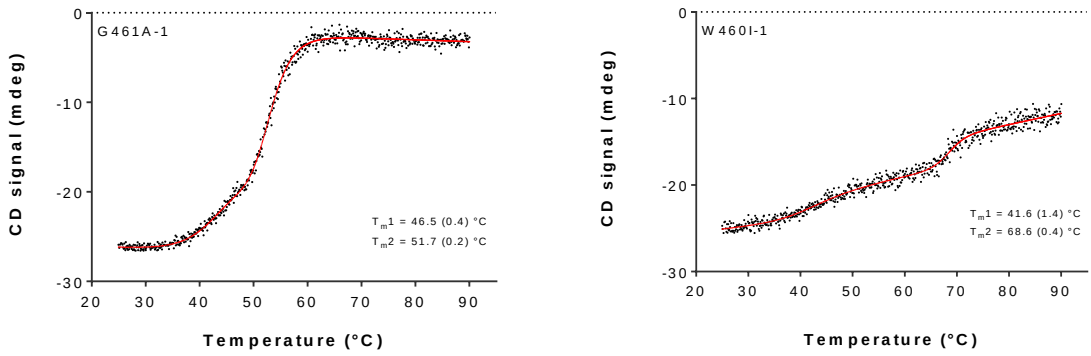

Figure 24. Melting curves of variants G461A and W460I.
The figure shows the melting curves of samples G461A-1 and W460I-1. In all, three samples were measured for each variant (see Appendix B for results). The curve of the G461A mutant was as expected. The asymmetry of the curve is due to an intermediate state. The measurements were performed in Mops buffer (25 mM Mops, 1 mM $MgSO_4$, pH 8.0). The CD signal was monitored at 222 nm with a temperature increase of 1°C/min in the range of 20-90°C.

3.6 Dimer-monomer equilibrium

To study the dimer-monomer equilibrium, enzyme dilution assays were performed under different conditions for both wild-type and G461A mutant. The activity of the W460I mutant was insufficient for measurements at such low concentrations. Activity measurements of all assays proved very difficult. The range of activity proved to be too wide to test all assays under the same conditions. Enzyme activity in samples of very low dimer concentrations was not sufficient for activity measurements. Twelve samples were prepared for each assay, but data is only shown for samples that had measurable activity. Results are given as relative specific activity of the enzyme (U/[E]), where the specific activity of the highest dimer concentration equals 1.

3.6.1 Dimer equilibrium of G461A mutant at pH 8.0 at 25°C

For the first assay, the dimer-monomer equilibrium of variant G461A was tested in 20 mM Tris buffer (20 mM Tris, 10 mM $MgCl_2$, pH 8.0). Two dilution series were made, with and without NaCl (Table 2.3). The series were done in duplicates and each data point was generally measured in duplicates. Enzyme activity was measured at pH 8.0 and 25°C.

Neither series showed decreased activity with decreased dimer concentration in the observed range of dimer concentration (Figure 25). It could indicate that the dimer dissociation happens at a dimer concentration outside the range tested in this assay.

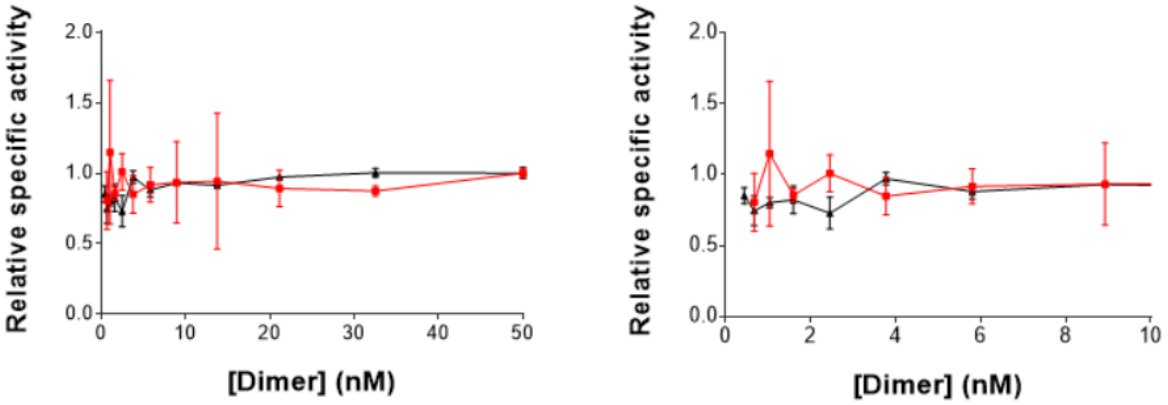

Figure 25. Dimer equilibrium of G461A mutant at pH 8.0.
The relative activity of the G461A mutant after dilution. Enzyme activity was measured at pH 8.0 and 25°C. Purified enzyme was diluted in Tris buffer (20 mM Tris, 10 mM $MgCl_2$, pH 8.0) and incubated at 10°C overnight. Assays were done in duplicates and each data point was generally measured in duplicates. The figure shows mean with standard deviation. The two plots are derived from the same data. The plot to the right is zoomed in on lower dimer concentration to aid the eye. ***Red:*** *500 mM NaCl was added to the buffer.* ***Black:*** *No salt was added to the buffer.*

3.6.2 Effect of NaCl and $MgCl_2$ on dimer equilibrium of G461A mutant at pH 8.0 at 10°C

For the second assay, the dimer-monomer equilibrium of variant G461A was tested in 50 mM Tris buffer (50 mM Tris, pH 8.0). Three dilution series were made, with 500 mM NaCl, with 10 mM $MgCl_2$ and with no salt added (Table 2.4). Enzyme activity was measured at pH 8.0 and 10°C. Data points were generally measured in triplicates.

Figure 26 shows the results of measurements in the second assay. The measurements for the series with NaCl show signs of possible dimer dissociation at concentrations below 1.5 nM. The series without NaCl did not show decreased activity with decreased dimer

concentration. Their absolute activity at lower dimer concentration was insufficient for activity measurements and could not be measured for concentrations below 1.5 nM.

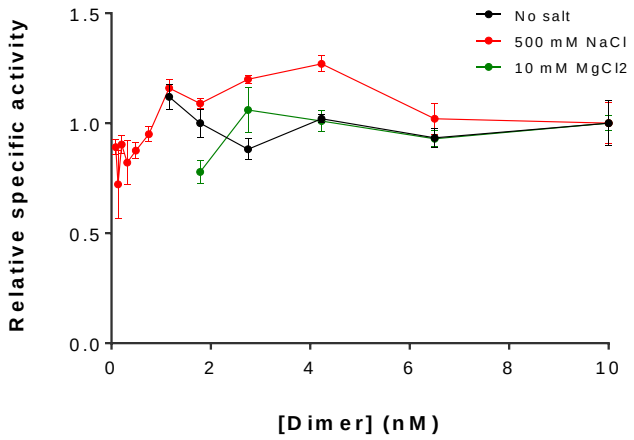

Figure 26. Effect of NaCl and $MgCl_2$ on dimer equilibrium of G461A mutant at pH 8.0.

The relative activity of the G461A mutant after dilution. Enzyme activity was measured at pH 8.0 and 10°C. Purified enzyme was diluted in 50 mM Tris buffer (50 mM Tris, pH 8.0) and incubated at 10°C overnight. Each data point was generally measured in triplicates. The figure shows mean with standard deviation. ***Red:*** *500 mM NaCl was added to the buffer.* ***Green:*** *10 mM $MgCl_2$ was added to the buffer.* ***Black:*** *No salt was added to the buffer.*

3.6.3 Effect of temperature and NaCl on dimer equilibrium of wild-type VAP at pH 8.0

For the third assay, the dimer-monomer equilibrium of wild-type VAP was tested in 50 mM Tris buffer (50 mM Tris, pH 8.0). Four dilution series were made to test the effect of temperature (10°C and 25°C) and to test the effect of NaCl at the different temperatures (Table 2.5). Enzyme activity of samples was measured at the same temperature as for the incubation of said sample. Activity was measured at pH 8.0 for all series and data points were generally measured in triplicates.

All series, except series 3c (with NaCl, 10°C), showed decreasing activity with decreased dimer concentration, indicating dimer dissociation. At 25°C, the addition of NaCl does not seem to affect the dimer-monomer equilibrium (Figure 27a). On the other hand, it does seem to stabilize the dimer at 10°C (Figure 27b). The dimer is more stable at 10°C than at 25°C regardless of NaCl (Figure 27c and d).

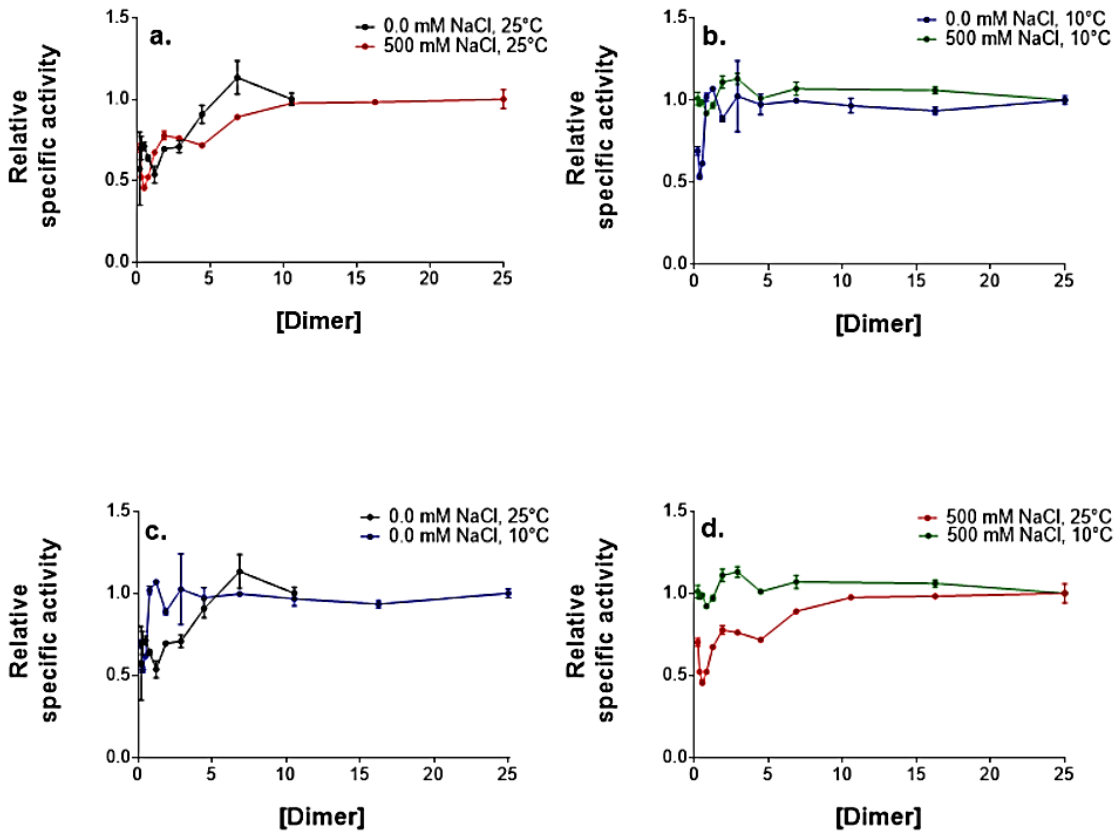

Figure 27. Effect of temperature and NaCl on dimer equilibrium of wild-type VAP at pH 8.0.

The relative activity of the G461A mutant after dilution. Enzyme activity was measured at pH 8.0. Purified enzyme was diluted in 50 mM Tris buffer (50 mM Tris, pH 8.0) and incubated overnight at either 10°C or 25°C. Activity measurements were performed at the same temperature as the sample was incubated at. Samples were incubated either with or without 500 mM NaCl Each data point was generally measured in triplicates. The figure shows mean with standard deviation. ***Green:*** *500 mM NaCl, 10°C.* ***Blue:*** *No NaCl, 10°C.* ***Red:*** *500 mM NaCl, 25°C.* ***Black:*** *No NaCl, 25°C.*

3.6.4 Dimer-monomer equilibrium of wild-type VAP and G461A mutant at pH 9.8

For the fourth assay, dimer-monomer equilibrium of wild-type VAP and G461A mutant was tested at 10°C and 25°C, at pH 9.8. The enzyme was diluted in Caps buffer (50 mM Caps, pH 9.8). two dilution series were made for each enzyme sample and tested at either 10°C or 25°C (Table 2.6). Enzyme activity of samples was measured at the same temperature as for

the incubation of said sample. Activity was measured at pH 9.8 for all series and data points were generally measured in triplicates.

All series showed similar trend in specific activity (Figure 28). The relative specific activity decreases rapidly for the first samples of the dilution series. The curves reach a plateau at lower dimer concentrations. The measurements were done for dimer concentrations of 10 nM or less. The loss of activity indicates dimer dissociation at dimer concentration above 6 nM.

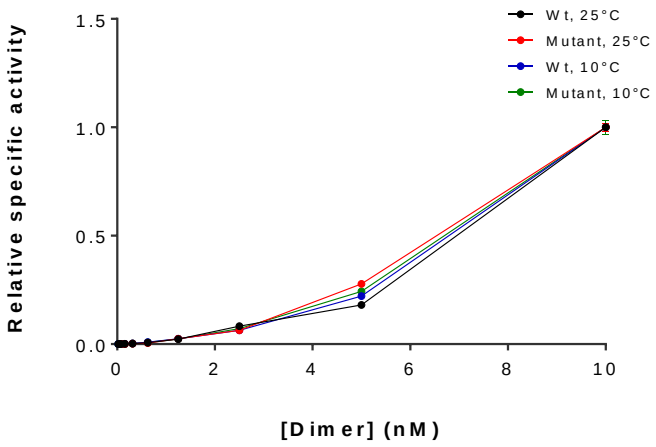

Figure 28. Dimer-monomer equilibrium of wild-type VAP and G461A mutant at pH 9.8.

The relative activity of wild-type VAP and the G461A mutant after dilution. Enzyme activity was measured at pH 9.8 at either 10°C or 25°C. Purified enzyme was diluted in 50 mM Caps buffer (50 mM Caps, pH 9.8) and incubated overnight at either 10°C or 25°C. Activity measurements were performed at the same temperature as the samples were incubated at. Each data point was generally measured in triplicates. The figure shows mean with standard deviation. ***Green:*** *Mutant, 10°C.* ***Red:*** *Mutant, 25°C.* ***Blue:*** *Wild-type, 10°C.* ***Black:*** *Mutant, 25°C.*

3.7 Enzyme inhibition by desthiobiotin

The inhibitory effect of DDB on VAP in Caps buffer (100 mM Caps, 1.0 mM $MgCl_2$, pH 9.8) was tested with wild-type enzyme. Three concentrations of DDB were analyzed – 2.5 mM, 0.25 mM and 0.05 mM. The effect of NaCl was also tested for 0.25 mM DDB. For control, assays were made without DDB. Each assay was performed once, and data points were measured in triplicates.

Desthiobiotin at 2.5 mM resulted in complete inhibition for all *p*NPP concentrations. At 0.05 mM, DDB did not result in a clear inhibition. Therefore, it was decided to use 0.25 mM DDB for further testing. All activity measurements were performed at pH 9.8 and 10°C.

3.7.1 Evidence of substrate inhibition

Figure 29 shows the results of the kinetic assays for VAP with or without DDB and NaCl. When the range of *p*NPP concentration exceeded 2.5 mM, the measurements showed evidence of substrate inhibition (see section 1.4.2 for definition). This seems to hold true for the enzyme whether it is incubated with or without DDB or NaCl. Figure 29a and b also show obvious inhibition by desthiobiotin in absence of NaCl, while Figure 29c and d show lack of inhibition by DDB at 500 mM NaCl (note the different scaling of Y axis for all figures).

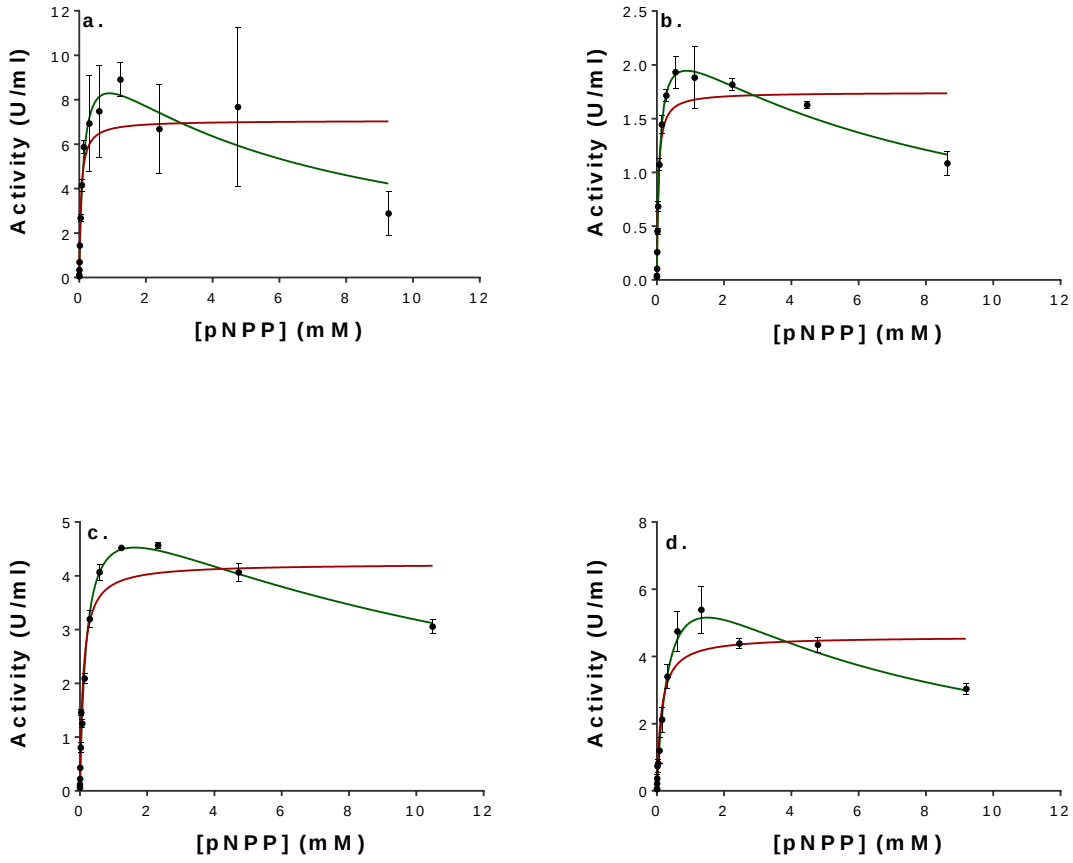

Figure 29. Evidence of substrate inhibition for wild-type VAP.
The graphs show enzyme activity of wild-type VAP measured at pH 9.8 and 10°C. pNPP was dissolved in 100 mM Caps containing 1.0 mM $MgCl_2$. Activity is shown as mean with standard deviation (N=3). The assays were either with or without DDB (2.5 mM) or NaCl (500 mM). For all assays, the measurements showed signs of substrate inhibition for pNPP concentration. ***a.*** *No NaCl, no DDB* ***b.*** *No NaCl, 0.25 mM DDB* ***c.*** *500 mM NaCl, no DDB* ***d.*** *500 mM NaCl, 0.25 mM DDB. Data was fitted both to the Michaelis-Menten equation (red line) and to substrate-inhibition equation (green line).*

Table 3.5 shows the kinetic parameters for VAP measured under the different condition. The parameters are derived either from the Michaelis-Menten equation or from the substrate-inhibition equation. For all samples, k_{cat} and K_m increase when substrate inhibition is assumed rather than classic Michaelis-Menten kinetics.

Table 3.5. Kinetic parameters of wild-type VAP.
Kinetic parameters of wild-type VAP were determined with data from Figure 29. The data was fitted both to the Michaelis-Menten equation and to substrate-inhibition equation. K_i describes the dissociation constant for binding of two substrate molecules to enzyme. The parameters are shown with standard error.

Sample	DDB	NaCl	Michaelis-Menten		Substrate inhibition		
			k_{cat} [s^{-1}]	K_m [mM]	k_{cat} [s^{-1}]	K_m [mM]	K_i [mM]
a	−	−	272	0.06	415	0.14	6.04
			(19)	(0.02)	(50)	(0.04)	(2.22)
b	+	−	67.2	0.05	90.2	0.09	8.63
			(2.4)	(0.01)	(2.6)	(0.01)	(0.95)
c	−	+	163	0.10	217	0.20	13.3
			(5)	(0.02)	(7)	(0.02)	(1.8)
d	+	+	177	0.13	299	0.38	5.91
			(9)	(0.03)	(23)	(0.06)	(1.12)

3.7.2 Desthiobiotin inhibition

To ease calculations, kinetic parameters for DDB inhibition were determined using *p*NPP concentrations below 1.0 mM. Inhibitor parameters were determined for DDB in absence of NaCl. The data for samples containing NaCl was insufficient to determine the effect of NaCl on DDB as an inhibitor.

Figure 30 shows a Lineweaver-Burk plot, a double reciprocal form of the Michaelis Menten equation, made with the data of samples **a** and **b** in Figure 29. The two lines intercept below the X axis and to the left of the Y axis. This indicates that DDB is a mixed inhibitor with $\alpha < 1$, i.e. a mixed inhibitor with higher affinity towards the $E \bullet S$ complex than free enzyme [29].

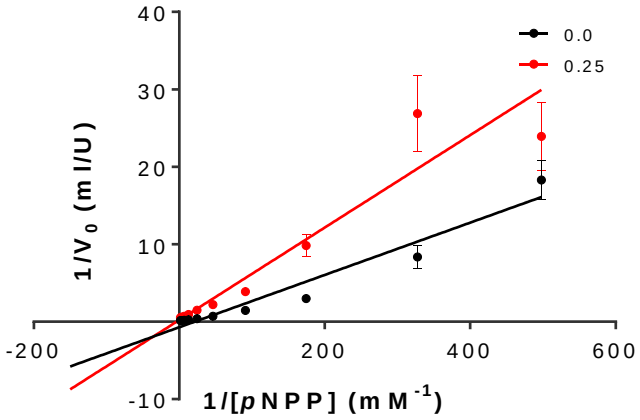

Figure 30 A Lineweaver-Burk plot for determining the type of inhibition.
The graph is a double reciprocal plot derived from the Michaelis-Menten equation. The plot shows the Lineweaver-Burk plot of the data from samples ***a*** *and* ***b*** *in figure 27. Activity is shown as mean with standard deviation (N=3). Sample* ***a*** *had no inhibitor added. Sample* ***b*** *had 0.25 mM DDB added. The two lines intercept to the left of the Y axis and below the X axis. This indicates that DDB is a mixed inhibitor with* $\alpha < 1$*, i.e. a mixed inhibitor that has higher affinity towards the E•S complex than free enzyme* [29].

Apparent kinetic parameters for VAP can be seen in Table 3.6. The parameters were determined using data for measured activity when *p*NPP < 1.0 mM. V_{max} and k_{cat} were lowered by 75% when the solution contained 0.25 mM DDB while K_m was lowered by 0.75%. K_i for DDB was determined to be 0.092 (0.055) mM and $\boldsymbol{\alpha}$ was determined to be 0.902 (0.738).

Table 3.6 Apparent kinetic parameters of VAP.
*Apparent kinetic parameters of wild-type VAP. The parameters were determined from activity for [*pNPP*] less than 1.0 mM. The parameters are shown with standard error.*

Sample	DDB	NaCl	$V_{max(app)}$ [U/ml]	$k_{cat(app)}$ [s^{-1}]	$K_{m(app)}$ [mM]
a	–	–	8.99 (0.66)	346 (25)	0.094 (0.020)
b	+	–	2.23 (0.04)	86 (2)	0.087 (0.005)

4 Discussions

4.1 Mutation of VAP with *p*ET11a plasmid vector

Five mutated plasmids were prepared – W460I, G461A, G461S, T462A and T462S. The mutagenesis was successful. DNA sequencing confirmed the presence of mutation in at least one strain of isolated plasmids, for each mutation. The sequencing also confirmed the absence of nonspecific mutations in the gene.

Agarose gel electrophoresis was used to determine the integrity of the purified plasmids (Figure 13). Almost all samples had a prominent band representing the supercoiled DNA. Most of the samples also exhibited a faint band above the supercoiled DNA bands, representing nicked plasmids. This is not unusual as the plasmids are nicked during DNA replication. This could be prevented by isolating the plasmids when the cultures are in the stationary phase. However, this was not important for the purpose of this study. The electrophoresis revealed two damaged samples, G461S-2 and T462A-1 (wells **b**6 and **c**1, respectively). The two strains chosen for this study were W460I-3 and G461A-2 (wells **a**4 and **b**3, respectively). Results from the DNA sequencing of the two strains can be seen in Appendix B.

Lemo21(DE3) competent *E. coli* cells were used to express mutated enzyme. *Strep*-Tactin® affinity columns were used to purify the enzyme samples. The samples were subjected to SDS-PAGE to confirm their purity (Figure 15). For the purified G461A enzyme sample (lane 5), a strong band was detected at 63.2 kDa. Hardly any impurities were detected in the sample. For the W460I mutant, a band was detected at 64.9 kDa. This band was much fainter than for the other mutant, indicating much lower protein concentration. The W460I mutant sample also had some impurities which might have affected the results of this study. Wild-type VAP has previously been characterized with a mass of 55 kDa for each monomer [13], slightly lower than the SDS-PAGE results indicated. The gel probably got too hot during the electrophoresis, as evident by inclining lanes. This skews the ladder bands' positions relative to the sample bands and makes size determination less reliable.

Protein concentration measurements confirmed the lesser concentration of the W460I samples compared to the G461A sample. 32.8 mg of G461A enzyme were obtained but only 0.01 mg of W460I enzyme. The yield of the purification of mutant G461A was 46% and the purification was 15.4-fold. The yield of the purification of mutant W460I was 37% and the purification was 42 600-fold. It should be noted, that because the W460I fractions were not pooled together, the activity and protein concentration were estimated from measurements on selected fractions. Therefore, these factors are not as reliable as the ones measured for the G461A mutant. It is likely that the protein concentration of variant W460I is underestimated.

All three purified enzyme samples of the SDS-PAGE gel clearly show a VAP band Figure 15), although it is not as prominent as the G461A band. The fact that samples before, after and in the middle of the active peak all show a VAP band indicates that the collected samples should contain a significant amount of enzyme. When protein concentration is underestimated, specific activity is overestimated, and purification is likewise overestimated.

Measurements of samples, taken at different points during the purification process, revealed that much of the G461A enzyme was lost in the flow-through after the lysate had been run through the column.

4.2 Enzyme kinetics

The enzymatic activity of the G461A mutant was found to be very similar to that of wild-type VAP, while the W460I mutation caused the enzyme to lose virtually all activity. Glycine and alanine differ only by one methyl group. Therefore, it is not surprising that the G → A mutation had little effect on the enzymes kinetic capability.

Tryptophan and isoleucine are both nonpolar amino acids, the difference between them is the aromatic side chain of tryptophan and the aliphatic branched side chain of isoleucine. W460 is situated on a short loop close to the binding site of a zinc ion. It has been theorized that W460 might participate in interactions with residues important in coordination of zinc ions[14].

The specific activity of purified G461A mutant was determined to be 6150 U/mg and 1590 U/mg for the W460I mutant. Wild-type VAP has previously been found to have specific activity of 3707 U/mg [13]. As noted earlier, the measurements for the calculation of specific activity were not very reliable for the W460I mutant. The specific activity of the W460I mutant is probably lower than the estimated value. This fact became apparent when the mutants Michaelis-Menten parameters were analyzed.

The mutants' activity was measured with varying *p*NPP concentrations to determine kinetic parameters. The results can be seen in Table 3.3, p.32. The W460I mutation caused the enzyme to lose 99.9% of its catalytic efficiency. K_m was increased 6-fold and k_{cat} was less than 0.25% of that of the wild-type. As mentioned before, SDS-PAGE showed some impurities in the sample. It could be, that the little activity measured is the result from these impurities. This particular mutation, has previously been found to render the enzyme completely inactive [14], supporting the idea that the activity was that of the impurities and not of the mutated enzyme. The G461A mutation did not seem to have any effect on the enzyme's kinetics when the data was fitted to the Michaelis-Menten equation.

Surprisingly, a substrate-inhibition inhibition model was a better fit for the G461A data than a normal Michaelis-Menten model (calculated with GraphPad Prism®). To the author's best knowledge, this has not before been recorded for *Vibrio* alkaline phosphatases.

Substrate inhibition has been recorded for more distantly related APs, e.g. hepatic AP [30], boar semen AP [31] and several different canine APs [32] and bovine APs [33].

Substrate-inhibition first became apparent when the inhibition of desthiobiotin was being studied (Figure 29). The inhibition was clear when *p*NPP concentrations reached above 2.5 nM. At pH 9.8, the inhibitor constant, K_i, for substrate inhibition is 6.04 mM *p*NPP. The inhibition seems to be weakened by the addition of 500 mM NaCl, where K_i has a value of 13.34 mM *p*NPP (Table 3.5, p.44). When enzyme activity of variant G461A was fitted to a substrate-inhibition model, the results indicated that the mutation might have some effect. However, relatively high standard deviations of values for both mutant and wild-type enzyme make comparison difficult.

4.3 Enzyme stability

The effect of urea on the mutants was analyzed, as well as the effect of temperature. Global temperature stability was determined with circular dichroism spectroscopy. The mutants' resistance to urea was determined with fluorescence spectroscopy and kinetic analysis after incubation in urea of various concentration.

Wild-type VAP has a reported melting temperature at 51.0°C. For this study, the melting curves were fitted to a three state T_m function to obtain two melting temperatures. T_m1 and T_m2 of the G461A mutant were determined to be 44.5°C and 53.1°C, respectively. For the W460I mutant, the two melting temperatures were determined to be 46.3°C and 68.1°C, respectively. As mentioned in section 3.2.2, the W460I purified enzyme had some impurities. It is highly likely that those impurities affected the results from the CD spectrometry since the melting curves indicate that even at the highest temperatures the sample still contained some folded protein.

The melting curve of the G461A mutant is as expected. The inactivation and unfolding of wild-type VAP has previously been shown to involve at least two intermediate states, an inactive dimer and unfolded monomers, before the enzyme is completely denatured [14]. In the study, the authors used fluorescence spectroscopy to prove the enzyme lost its activity before it was denatured by urea. This current study has shown that the same applies to the G461A mutant, which has lost most of its activity before a change in λ_{max} could be detected (Figure 31a). This is in accordance with the obvious asymmetry of the G461A variants melting curve (Figure 24). A two-state unfolding protein would have a symmetric melting curve and one melting point. Melting temperatures of the G461A variant were estimated at 44.5°C and 53.1°C.

For the W460I mutant, a change in λ_{max} was also detected, although not as great as for the G461A mutant. Activity measurements also indicated that the W460I variant could withstand higher concentrations of urea (Figure 31b). Again, as mentioned earlier, the absolute activity of the W460I mutant was very low and might have been the result of impurities in the sample. As mentioned in the previous section, the mutation has previously

been reported to render the enzyme completely inactive. Thus, it is unlikely that the low activity was because of inhibition by the impurities. It is rather likely that the impurities were some sort of enzymes with vague phosphatase activity.

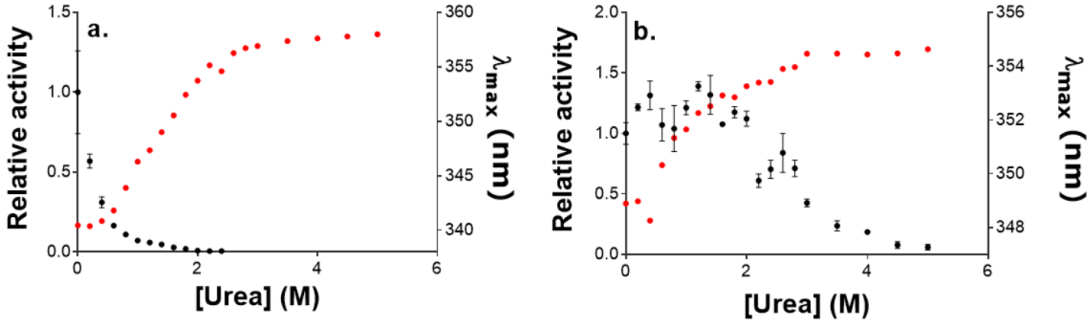

Figure 31. Deactivation of the mutants compared to changes in quaternary structure after incubation in urea.
The samples were incubated in various urea concentrations overnight at 10°C. Change in λ_{max} was compared to the decrease of inactivity. ***a.*** *Mutant G461A. The enzyme had lost about 75% of its activity when a change in λ_{max} was detected.*

4.4 Dimer-monomer equilibrium

The G461A mutated enzyme was diluted to assess the dimer-monomer equilibrium. The results of the assays were not conclusive, and it was not possible to calculate the dimer dissociation constant, K_d, as was previously done [28]. However, the results offered ideas of possible effects of the dimer dilutions. At least, it is clear that the dimer is extremely stable at pH 8.

For the first assay, the measurements showed no signs of decreased activity with decreased dimer concentration and the addition of 500 mM NaCl did not have any effect (Figure 25). Wild-type VAP has previously been shown to have K_d = 7.3 nM under the same conditions [28]. However, the wild type samples were incubated at 25°C whereas the samples of this study were incubated at 10°C. The enzyme is cold-adapted and highly heat-labile, with respect to its activity. It is possible that the dimer is also more stable at cold temperatures and the dimer concentrations tested were not low enough to observe the dissociation.

For the second assay, the samples were also incubated at 10°C. For this assay, the dilution series started with 10 nM dimer concentration while the first assay started with 50 nM dimer. In this assay, the effect of $MgCl_2$ was also tested. The measurements of samples with 500 mM NaCl added showed signs of dimer dissociation at concentrations below 1.5 nM (Figure 26). However, this is unclear due to high uncertainty of the measurements. At very low concentrations, the enzyme's absolute activity was very low which made measurements difficult. Since NaCl is known to increase the activity of VAP, the samples without NaCl had even less absolute activity and could not be measured for concentrations below 1.5 nM. Above 1.5 nM, neither of these samples showed signs of dimer dissociation

For the third assay, the dimer-monomer equilibrium of wild-type VAP was tested (Figure 27). The assay tested the effect of both temperature and 500 mM NaCl with four dilution series. All series showed signs of dimer dissociation, except the series with NaCl incubated at 10°C. For both series incubated at 25°C, the decrease in activity started at 10 nM dimer concentration. That does not contradict the previously determined K_d of 7.3 nM. For the series incubated at 10°C without NaCl, the decrease in activity started at 2 nM, comparable to the results of the second assay. The third assay did not reveal a decrease in activity of the series incubated in NaCl at 10°C, although an identical sample in the second assay did exhibit some loss of activity at very low dimer concentrations. For the third assay, the most diluted sample had dimer concentration of 0.22 nM while the enzyme sample of the second assay was diluted down to 0.087 nM. The dimer dissociation, observed in the second assay, could possibly occur at too low of a concentration to be observed in the third assay. Therefore, it is possible that NaCl has some stabilizing effect at 10°C. However, it does not seem to stabilize the dimer at 25°C. It could also be that the wild-type enzyme's dimer is more stable than the mutant dimer. It is also apparent that the dimer is more stable at 10°C than at 25°C.

For the fourth assay, the dimer-monomer equilibrium was tested at pH 9.8 and the mutant compared to the wild-type (Figure 28). Samples were incubated at 10°C and 25°C to test the effect of temperature. The measurements were done for dimer concentrations of 10 nM or less. All series had almost identical curves. Activity decreased rapidly between the first samples and the decrease reached a plateau at lower dimer concentrations. It is possible that the decrease in activity follows a sigmoidal curve with plateaus below 1.5 nM and somewhere above 10 nM. That would be consistent with the theory that the enzyme exists in an equilibrium between the monomeric and dimeric state. The measurements indicated that dimer dissociation happens above 6 nM. However, it is not possible to tell if K_d at pH 9.8 is similar to the one recorded for pH 8.0 (7.3 nM).

4.5 Enzyme inhibition by desthiobiotin

When *p*NPP concentrations reached above 2.5 mM, substrate inhibition became apparent. At pH 9.8, the inhibitor constant (K_i) for substrate inhibition is 6.0 mM *p*NPP. The inhibition

seems to be weakened by the addition of 500 mM NaCl, where K_i has a value of 13.3 mM *p*NPP. To the author's best knowledge, substrate inhibition has not been recorded for alkaline phosphatases from species of *Vibrio*. Substrate inhibition has been recorded for more distantly related APs [30,31,34].

Desthiobiotin is used to elute VAP from *Strep*-Tactin® affinity columns. Recently, images of crystal structures have shown that desthiobiotin aligns to the W460 side-chain of the enzyme and possibly act as an inhibitor. Therefore, it was important to determine the inhibitory effect of DDB on VAP. The results indicate that DDB is a mixed inhibitor with higher affinity towards the E•S complex that free enzyme. The binding site is not in the enzyme's active site which means that DDB is an allosteric inhibitor. However, W460 is close to the active site and it is possible that DDB acts as a competitive inhibitor by preventing substrate binding because of electrostatic forces or steric hindrance.

Eq. 4 shows how this type of inhibition affects kinetic parameters. Values of V_{max} and K_m are both lowered by the inhibitor, but not by the same factor. The ratio of V_{max}/K_m decreases with increasing $[I]$ and the lines of a Lineweaver-Burk plot intersect to the left of the Y axis. Weather the lines converge above or below the X axis depends on the value of α. In this equation, K_i describes the affinity of inhibitor toward free enzyme and αK_i describes its affinity toward the E•S complex. Thus, when α > 1, the inhibitor shows higher affinity toward the free enzyme. When α < 1, the inhibitor shows higher affinity toward the $E \bullet S$ complex. When α = 1 is known as a special case called non-competitive inhibition where the inhibitor has the same affinity towards free enzyme and the $E \bullet S$ complex and K_m is not affected [29]. K_i was determined to be 0.091 mM DDB and α was determined to be 0.902.

$$v = \frac{\frac{V_{max}}{\left(1 + \frac{[I]}{\alpha K_i}\right)}[S]}{[S] + K_m\left(\frac{1 + \frac{[I]}{K_i}}{1 + \frac{[I]}{\alpha K_i}}\right)} \qquad Eq.4$$

Inhibition calculations can rapidly become very complicated. This was true for this study where the enzyme also exhibited properties of substrate inhibition. To ease calculations, it was decided to determine K_i and α using only data for measured activity when *p*NPP < 1.0 mM. This was done so the data could be fitted easily to the Michaelis-Menten equation, since results indicated that the enzyme followed classic Michaelis-Menten kinetics in that range. However, more experiments would have to be performed to validate that theory and obtain more accurate kinetic constants.

The measurements were performed with 0.25 mM DDB, a 10-fold dilution from the concentration used when eluting VAP from the affinity columns. At this concentration, V_{max} and k_{cat} were lowered by 75% compared to samples without DDB. K_m was lowered by 0.75%. However, purified enzyme samples are always diluted before measurements – usually by a factor of at least 1000 – minimizing the effect of DDB.

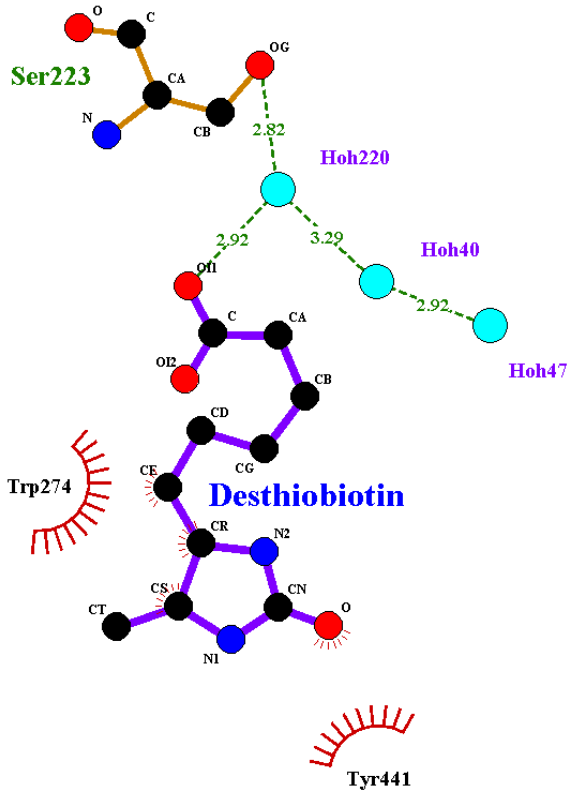

Figure 32. d-Desthiobiotin might interact with VAP mainly through hydrophobic interactions

An image of d-Desthiobiotin depicting how it might interact with VAP as an inhibitor. The interactions seem to be mostly hydrophobic, although there is a possibility of hydrogen binding to Ser223 through water molecules (The image was drawn in LigPlot+ by Jens G. Hjörleifsson).

5 What next?

The results of this study are in accordance with the theory that VAP goes through intermediate states while it unfolds. This is quite interesting and further experiments would have to be performed to determine how the protein unfolds. How that can be done is, however, not clear. Size-exclusion chromatography has previously been used [14] but poor resolution means that the results are often biased. Another problem with size-exclusion chromatography is that the enzyme could interact with the resin and that the sample is not necessarily homogeneous in concentration throughout the column. Fluorescence spectroscopy can be used to detect changes in an enzymes structure, but only if the enzyme has Trp or Tyr residues that are situated so that their environment changes when the protein unfolds. For VAP, it is not possible to monitor the change in dimer dissociation with fluorescence. CD spectroscopy follows the change in circular dichroism of the enzyme and is able to detect slight changes in the secondary structure. The biggest problem with this method is the difficulty of fitting the data to an appropriate curve. The slightest error in the fit can change the output values drastically. This is though not impossible. The enzyme dilution assays performed in this study, as well as in previous studies, have shown that dimer dissociation might be monitored in that way. Yet, these measurements have also proven to be difficult and have only given an idea of what might be happening. Perhaps it is possible to optimize this method to test for dimer dissociation.

This study revealed that desthiobiotin is an inhibitor of VAP. How exactly, is not clear and further studies would have to be done to characterize the interaction of DDB with VAP. It would be interesting to mutate Trp274, Tyr411 or Ser223 (the residues shown to possibly interact with the molecule) and see if it has any effect on the inhibition. Since DDB is present to some extent in almost every single enzyme sample, it is important to characterize the inhibition and confirm if DDB might have any effect on the results or not.

A surprising result from the kinetic studies is the substrate-inhibition of VAP. Few studies exist on AP substrate inhibition and to the author's best knowledge, this is the first to report *Vibrio* AP substrate inhibition. Not long ago, researchers disagreed on how common or rare this type of inhibition was which might explain the lack of research. It is also possible that the substrate inhibitions happen at such a high level of substrate that researchers rarely encounter it by accident. However, it has become clear that substrate inhibition can be essential for a number of biological phenomena.

References

[1] R.B. Silverman, Organic Chemistry of Enzyme-Catalyzed Reaction, 2nd ed., Elsevier, Austin, 2002.

[2] D.L. Nelson, M.M. Cox, 6. Enzymes, in: Princ. Biochem., 6th ed., W. H. Freeman, New York, 2013: pp. 189–242.

[3] A. Bar-Even, E. Noor, Y. Savir, W. Liebermeister, D. Davidi, D.S. Tawfik, R. Milo, The moderately efficient enzyme: Evolutionary and physicochemical trends shaping enzyme parameters, Biochemistry. 50 (2011) 4402–4410. doi:10.1021/bi2002289.

[4] H. Bisswanger, Enzyme Kinetics: Principles and Methods, 3rd ed., Wiley-VCH, 2017.

[5] S.C.L. Kamerlin, P.K. Sharma, R.B. Prasad, A. Warshel, Why nature really chose phosphate, Q. Rev. Biophys. 46 (2013) 1–132. doi:10.1017/S0033583512000157.

[6] C. Lad, N.H. Williams, R. Wolfenden, The rate of hydrolysis of phosphomonoester dianions and the exceptional catalytic proficiencies of protein and inositol phosphatases, Proc. Natl. Acad. Sci. U. S. A. 100 (2003) 5607–5610. doi:10.1073/pnas.0631607100.

[7] G.K. Schroeder, C. Lad, P. Wyman, N.H. Williams, R. Wolfenden, The time required for water attack at the phosphorus atom of simple phosphodiesters and of DNA, Proc. Natl. Acad. Sci. U. S. A. 103 (2006) 4052–4055. doi:10.1073/pnas.0510879103.

[8] E.E. Kim, H.W. Wyckoff, Reaction mechanism of alkaline phosphatase based on crystal structures, J. Mol. Biol. 218 (1991) 449–464. doi:10.1016/0022-2836(91)90724-K.

[9] R. Helland, R.L. Larsen, B. Ásgeirsson, The 1.4 Å crystal structure of the large and cold-active Vibrio sp. alkaline phosphatase, Biochim. Biophys. Acta - Proteins Proteomics. 1794 (2009) 297–308. doi:10.1016/j.bbapap.2008.09.020.

[10] J.L. Millán, Alkaline phosphatases, Purinergic Signal. 2 (2006) 335–341. doi:10.1007/s11302-005-5435-6.

[11] B. Stec, K.M. Holtz, E.R. Kantrowitz, A revised mechanism for the alkaline phosphatase reaction involving three metal ions, J. Mol. Biol. 299 (2000) 1303–1311. doi:10.1006/jmbi.2000.3799.

[12] K.M. Holtz, E.R. Kantrowitz, The mechanism of the alkaline phosphatase reaction: Insights from NMR, crystallography and site-specific mutagenesis, FEBS Lett. 462 (1999) 7–11. doi:10.1016/S0014-5793(99)01448-9.

[13] J.B. Hauksson, Ó.S. Andrésson, B. Ásgeirsson, Heat-labile bacterial alkaline phosphatase from a marine Vibrio sp, Enzyme Microb. Technol. 27 (2000) 66–73. doi:10.1016/S0141-0229(00)00152-6.

[14] J.G. Hjörleifsson, B. Ásgeirsson, Cold-active alkaline phosphatase is irreversibly transformed into an inactive dimer by low urea concentrations, BBA - Proteins Proteomics. 1864 (2016) 755–765. doi:10.1016/j.bbapap.2016.03.016.

[15] E. Papaleo, G. Renzetti, G. Invernizzi, B. Ásgeirsson, Dynamics fingerprint and inherent asymmetric flexibility of a cold-adapted homodimeric enzyme. A case study of the Vibrio alkaline phosphatase, Biochim. Biophys. Acta - Gen. Subj. 1830 (2013) 2970–2980. doi:10.1016/j.bbagen.2012.12.011.

[16] M.F. Hoylaerts, L. Ding, S. Narisawa, S. Van kerckhoven, J.L. Millán, Mammalian alkaline phosphatase catalysis requires active site structure stabilization via the N-

terminal amino acid microenvironment, Biochemistry. 45 (2006) 9756–9766. doi:10.1021/bi052471+.
[17] G. Feller, Psychrophilic Enzymes: From Folding to Function and Biotechnology, Scientifica (Cairo). 2013 (2013) 1–28. doi:10.1155/2013/512840.
[18] A. Cornish-Bowden, Why is uncompetitive inhibition so rare?. A possible explanation, with implications for the design of drugs and pesticides, FEBS Lett. 203 (1986) 3–6. doi:10.1016/0014-5793(86)81424-7.
[19] N.K. Ghosh, W.H. Fishmas, L-Phenylalanine inhibition of rat intestinal alkaline phosphatase: A homosteric phenomenon, Arch. Biochem. Biophys. 126 (1968) 700–706. doi:10.1016/9993-9861(68)90457-8.
[20] P.W. Kühl, Excess-substrate inhibition in enzymology and high-dose inhibition in pharmacology: a reinterpretation [corrected]., Biochem. J. 298 (1994) 171–180. doi:10.1042/bj2980171.
[21] P.M. Kaiser, Substrate inhibition as a problem of non-linear steady state kinetics with monomeric enzymes, J. Mol. Catal. 8 (1980) 431–442. doi:10.1016/0304-5102(80)80082-4.
[22] M.C. Reed, A. Lieb, H.F. Nijhout, The biological significance of substrate inhibition: A mechanism with diverse functions, BioEssays. 32 (2010) 422–429. doi:10.1002/bies.200900167.
[23] D.S. Goodsell, A.J. Olson, S s p f, Annu. Rev. Biophys. Biomol. Struct. 29 (2000) 105–153. doi:10.1146/annurev.biophys.29.1.105.
[24] S. Sultana, H.A. Al-Shawafi, S. Makita, M. Sohda, N. Amizuka, R. Takagi, K. Oda, An asparagine at position 417 of tissue-nonspecific alkaline phosphatase is essential for its structure and function as revealed by analysis of the N417S mutation associated with severe hypophosphatasia, Mol. Genet. Metab. 109 (2013) 282–288. doi:10.1016/j.ymgme.2013.04.016.
[25] T.G.M. Schmidt, A. Skerra, The Strep-tag system for one-step purification and high-affinity detection or capturing of proteins, Nat. Protoc. 2 (2007) 1528–1535. doi:10.1038/nprot.2007.209.
[26] Z. Zaman, R.L. Verwilghen, Quantitation of proteins solubilized in sodium dodecyl sulfate-mercaptoethanol-tris electrophoresis buffer, Anal. Biochem. 100 (1979) 64–69. doi:10.1016/0003-2697(79)90110-6.
[27] M.M. Bradford, A rapid and sensitive method for the quantitation of microgram quantities of protein utilizing the principle of protein-dye binding, Anal. Biochem. 72 (1976) 248–254. doi:10.1016/0003-2697(76)90527-3.
[28] B. Hjörleifsson, Jens G.Ásgeirsson, PH-Dependent Binding of Chloride to a Marine Alkaline Phosphatase Affects the Catalysis, Active Site Stability, and Dimer Equilibrium, Biochemistry. 56 (2017) 5075–5089. doi:10.1021/acs.biochem.7b00690.
[29] R.A. Copeland, Evaluation of Enzyme Inhibitors in Drug Discovery, 2nd ed., Wiley-Interscience, Hoboke, N.J., 2013.
[30] T. Komoda, Y. Sakagishi, Komoda1976.pdf, Biochim. Biophys. Acta. 438 (1976) 138–152. doi:10.1016/0005-2744(76)90230-8.
[31] J. Glogowski, D.R. Danforth, A. Ciereszko, Inhibition of alkaline phosphatase activity of boar semen by pentoxifylline, caffeine, and theophylline., J. Androl. 23 (2002) 783–792. doi:10.1002/j.1939-4640.2002.tb02334.x.
[32] H. van Belle, Kinetics and inhibition of alkaline phosphatases from canine tissues, Biochim. Biophys. Acta. 289 (1972) 158–168. doi:10.1016/0005-2744(72)90118-0.
[33] S.P. Coburn, J.D. Mahuren, M. Jain, Y. Zubovic, F. Wayne, S. Developmental,

Alkaline Phosphatase (EC 3.1.3.1) in Serum is inhibited by Physiological Concentrations of Inorganic Phosphate *, 83 (1998) 3951–3957. doi:10.1210/jcem.83.11.5288.

[34] C. Arsenis, J. Rudolph, M.H. Hackett, Resolution, purification and characterization of the orthophophate releasing activities from fracture callus calcifying cartilage, Biochim. Biophys. Acta. 391 (1975) 301–315. doi:10.1016/0005-2744(75)90254-5.

Appendix A

Mediums

All mediums were sterilized in an autoclave.

SOB medium
2% w/v tryptone
0.5% w/v Yeast extract
10 mM NaCl
2.5 mM KCl
10 mM $MgCl_2$
10 mM $MgSO_4$

SOC medium
SOB medium containing 20 mM glucose.

LB agar plates
1.5% w/v agar
10 g/l Tryptone
5 g/l Yeast extract
10 g/l NaCl

Lamp agar plates
LB agar plates containing 100 μg/ml ampicillin.

Lamp + chloramphenicol agar plates
LB agar plates containing 100 μg/ml ampicillin and 30 μg/ml chloramphenicol.

LB medium
10 g/l Tryptone
5 g/l Yeast extract
10 g/l NaCl

Lamp medium
LB medium containing 100 μg/ml ampicillin.

LampCHL
LB medium containing 100 μg/ml ampicillin and 30 μg/ml chloramphenicol.

Buffers

TAE buffer
(Agarose gel electrophoresis)

4 mM Tris
2 mM Acetic acid
0.1 mM EDTA
pH 8.0

Lysis buffer
(Enzyme purification)

20 mM Tris
10 mM $MgCl_2$
0.01% (w/v) Triton X-100
pH 8.0

TMC buffer
(Affinity chromatography and dimer-monomer equilibrium)

20 mM Tris
10 mM $MgCl_2$
pH 8.0

Buffer R (10x HABA buffer)
(Affinity chromatography)

1 M Tris-Cl
1.5 M NaCl
10 mM EDTA
10 mM HABA (hydroxy-azophenyl-benzoic acid)

HABA buffer
(Affinity chromatography)

1 part Buffer R dissolved in 10 parts TMC buffer

Washing buffer
(Affinity chromatography)

TMC containing 0.15 M NaCl

Elution buffer
(Affinity chromatography)

TMC containing 0.15 M NaCl, 15% ethylene glycol and 2.5 mM desthiobiotin

DAE buffer
(Standard kinetic assay)

0.1 M Diethanolamine
1 mM $MgCl_2$
pH 9.8

Caps buffer
(Determination of kinetic parameters)

100 mM Caps
500 mM NaCl
1.0 mM $MgCl_2$
pH 9.8

50 mM Caps buffer
(Dimer-monomer equilibrium)

50 mM Caps
pH 9.8

Tris buffer
(Dimer-monomer equilibrium)

50 mM Trizma® (TRIS base)
pH 8.0

Mops buffer
(Stability measurements)

25 mM Mops
1 mM $MgSO_4$
pH 8.0

Viðauki B

DNA sequencing data

QuikChange® site-directed mutagenesis was used to introduce mutations into the VAP gene. Three clones for each variant were selected and sent for sequencing. The DNA sequencing data was analysed with ApE – A Plasmid Editor (v2.0.53c). Following is the sequence and analysis for the positive clones, of the G461A and W460I variants, selected for further studies. The upper lines represent the wilt-type sequence and the lower lines represent the mutant sequence. Place of mutation is highlighted with red.

Variant G461A (strain 2)

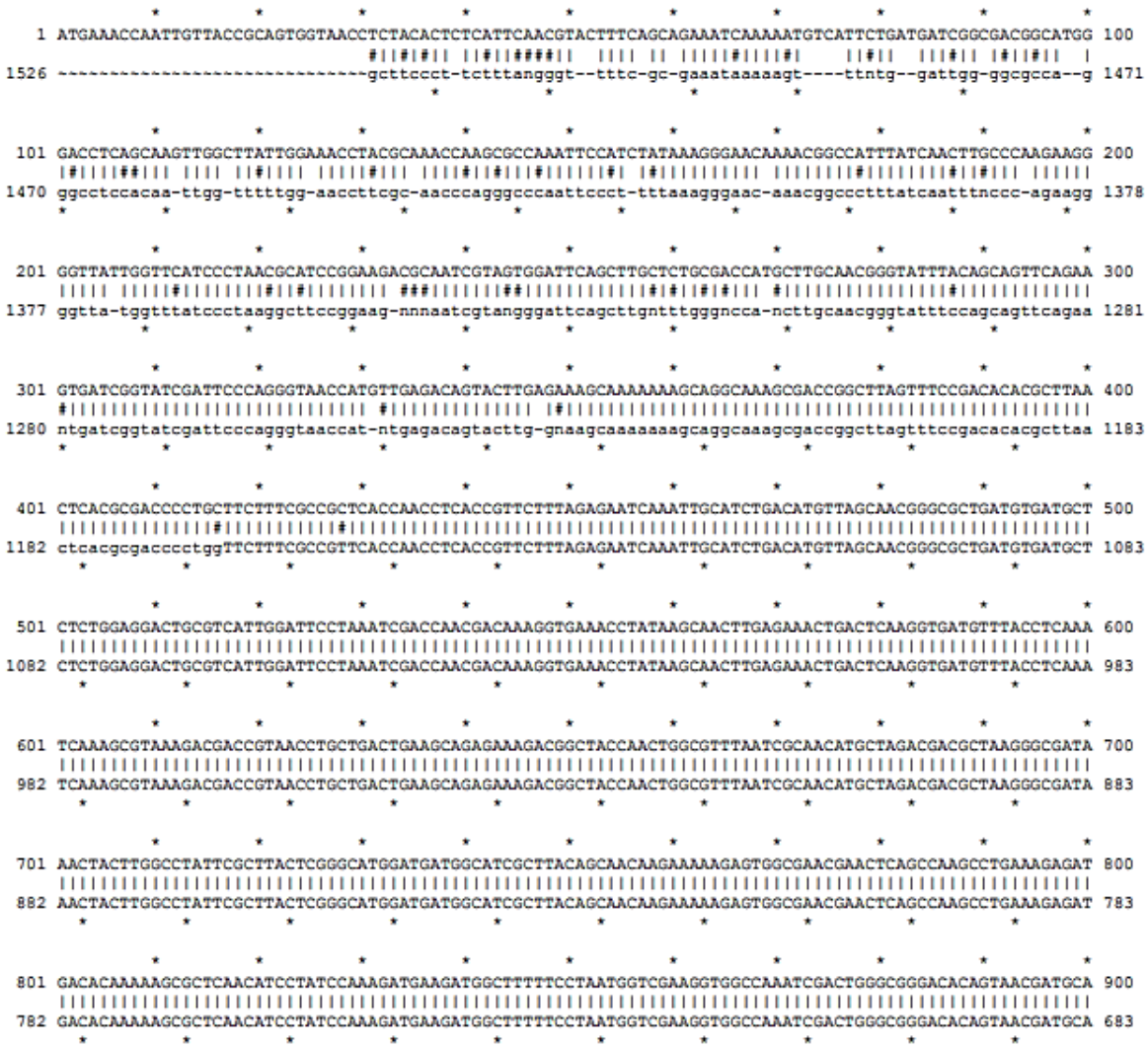

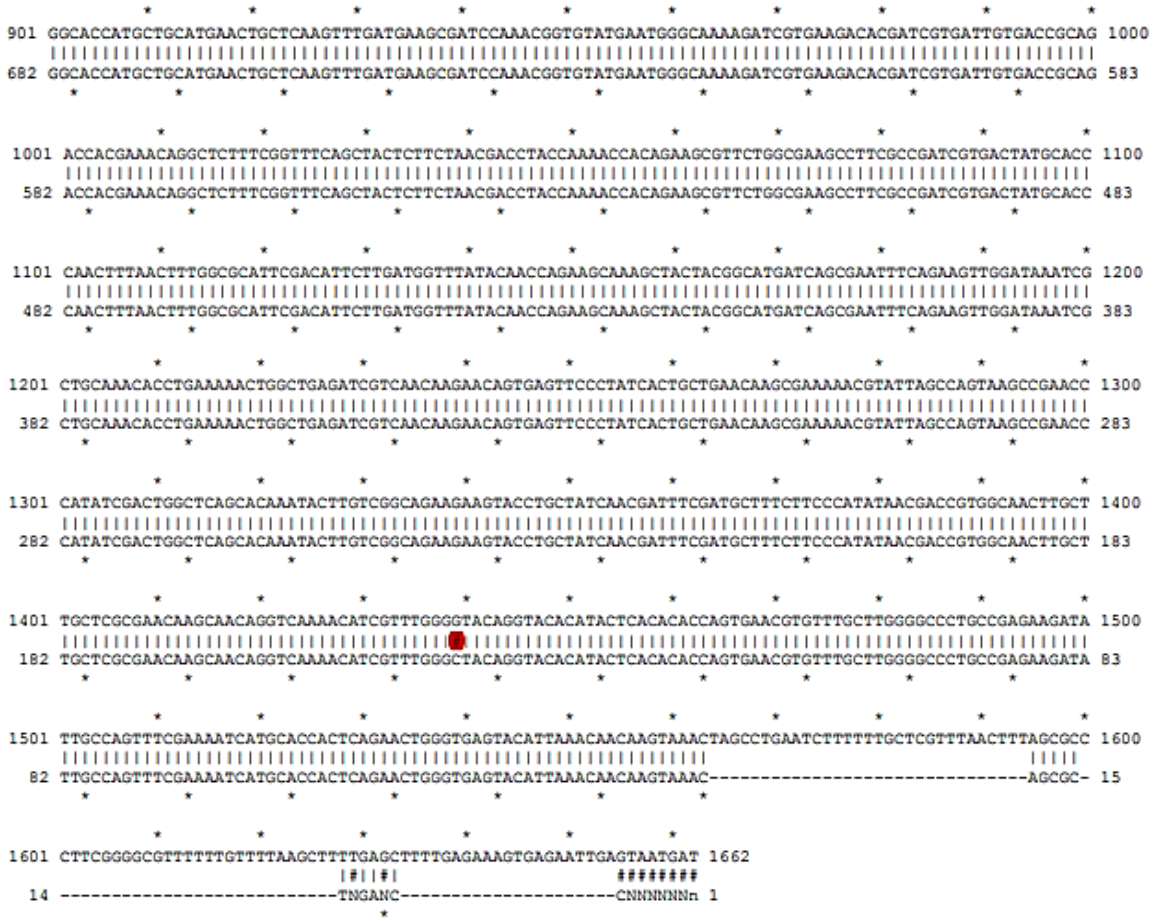
901 GGCACCATGCTGCATGAACTGCTCAAGTTTGATGAAGCGATCCAAACGGTGTATGAATGGGCAAAAGATCGTGAAGACACGATCGTGATTGTGACCGCAG 1000
682 GGCACCATGCTGCATGAACTGCTCAAGTTTGATGAAGCGATCCAAACGGTGTATGAATGGGCAAAAGATCGTGAAGACACGATCGTGATTGTGACCGCAG 583
1001 ACCACGAAACAGGCTCTTTCGGTTTCAGCTACTCTTCTAACGACCTACCAAAACCACAGAAGCGTTCTGGCGAAGCCTTCGCCGATCGTGACTATGCACC 1100
582 ACCACGAAACAGGCTCTTTCGGTTTCAGCTACTCTTCTAACGACCTACCAAAACCACAGAAGCGTTCTGGCGAAGCCTTCGCCGATCGTGACTATGCACC 483
1101 CAACTTTAACTTTGGCGCATTCGACATTCTTGATGGTTTATACAACCAGAAGCAAAGCTACTACGGCATGATCAGCGAATTTCAGAAGTTGGATAAATCG 1200
482 CAACTTTAACTTTGGCGCATTCGACATTCTTGATGGTTTATACAACCAGAAGCAAAGCTACTACGGCATGATCAGCGAATTTCAGAAGTTGGATAAATCG 383
1201 CTGCAAACACCTGAAAAACTGGCTGAGATCGTCAACAAGAACAGTGAGTTCCCTATCACTGCTGAACAAGCGAAAAACGTATTAGCCAGTAAGCCGAACC 1300
382 CTGCAAACACCTGAAAAACTGGCTGAGATCGTCAACAAGAACAGTGAGTTCCCTATCACTGCTGAACAAGCGAAAAACGTATTAGCCAGTAAGCCGAACC 283
1301 CATATCGACTGGCTCAGCACAAATACTTGTCGGCAGAAGAAGTACCTGCTATCAACGATTTCGATGCTTTCTTCCCATATAACGACCGTGGCAACTTGCT 1400
282 CATATCGACTGGCTCAGCACAAATACTTGTCGGCAGAAGAAGTACCTGCTATCAACGATTTCGATGCTTTCTTCCCATATAACGACCGTGGCAACTTGCT 183
1401 TGCTCGCGAACAAGCAACAGGTCAAAACATCGTTTGGGGTACAGGTACACATACTCACACACCAGTGAACGTGTTTGCTTGGGGCCCTGCCGAGAAGATA 1500
182 TGCTCGCGAACAAGCAACAGGTCAAAACATCGTTTGGGCTACAGGTACACATACTCACACACCAGTGAACGTGTTTGCTTGGGGCCCTGCCGAGAAGATA 83
1501 TTGCCAGTTTCGAAAATCATGCACCACTCAGAACTGGGTGAGTACATTAAACAACAAGTAAACTAGCCTGAATCTTTTTTGCTCGTTTAACTTTAGCGCC 1600
82 TTGCCAGTTTCGAAAATCATGCACCACTCAGAACTGGGTGAGTACATTAAACAACAAGTAAAC----------AGCGC- 15
1601 CTTCGGGGCGTTTTTTGTTTTAAGCTTTTGAGCTTTTGAGAAAGTGAGAATTGAGTAATGAT 1662
14 ----------TNGANC----------CNNNNNNn 1

Variant W460I (strain 3)

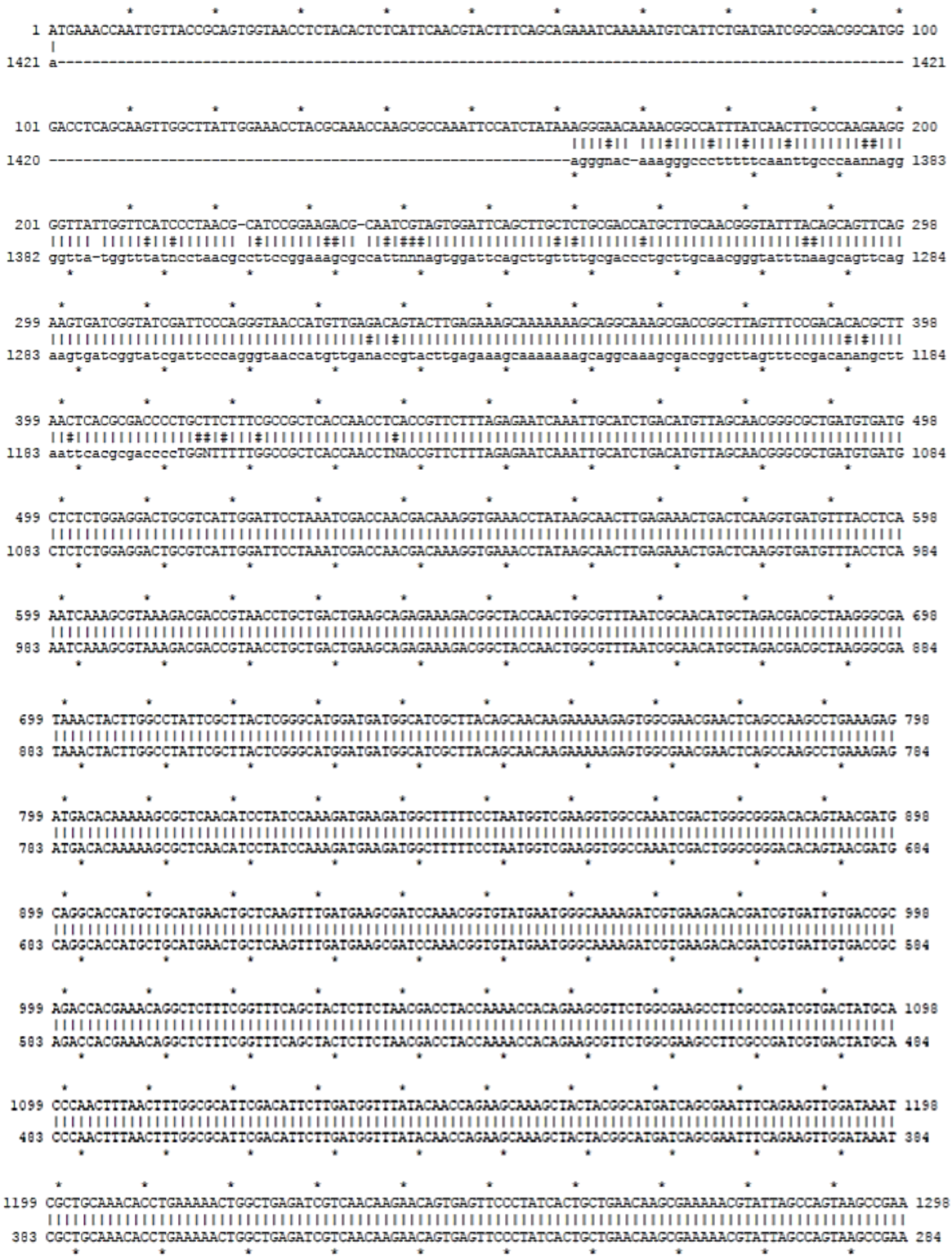

```
1299 CCCATATCGACTGGCTCAGCACAAATACTTGTCGGCAGAAGAAGTACCTGCTATCAACGATTTCGATGCTTTCTTCCCATATAACGACCGTGGCAACTTG 1398
     ||||||||||||||||||||||||||||||||||||||||||||||||||||||||||||||||||||||||||||||||||||||||||||||||||||
 283 CCCATATCGACTGGCTCAGCACAAATACTTGTCGGCAGAAGAAGTACCTGCTATCAACGATTTCGATGCTTTCTTCCCATATAACGACCGTGGCAACTTG 184

1399 CTTGCTCGCGAACAAGCAACAGGTCAAAACATCGTTTGGGGTACAGGTACACATACTCACACACCAGTGAACGTGTTTGCTTGGGGCCCTGCCGAGAAGA 1498
     ||||||||||||||||||||||||||||||||||###||||||||||||||||||||||||||||||||||||||||||||||||||||||||||||||
 183 CTTGCTCGCGAACAAGCAACAGGTCAAAACATCGTTATTGGTACAGGTACACATACTCACACACCAGTGAACGTGTTTGCTTGGGGCCCTGCCGAGAAGA 84

1499 TATTGCCAGTTTCGAAAATCATGCACCACTCAGAACTGGGTGAGTACATTAAACAACAAGTAAACTAGCCTGAATCTTTTTTGCTCGTTTAACTTTAGCG 1598
     ||||||||||||||||||||||||||||||||||||||||||||||||||||||||||#||||||||||||                    ||||
  83 TATTGCCAGTTTCGAAAATCATGCACCACTCAGAACTGGGTGAGTACATTAAANAACAAGTAAAC----------------------------AGCG 15

1599 CCCTTCGGGGCGTTTTTTGTTTTAAGCTTTTGAGCTTTTGAGAAAGTGAGAATTGAGTAATGAT 1662
     |                |##|                          #########
  14 C----------------TNNA----------------------------NNNNNNNNnn 1
```

Standard curve for determination of protein concentration

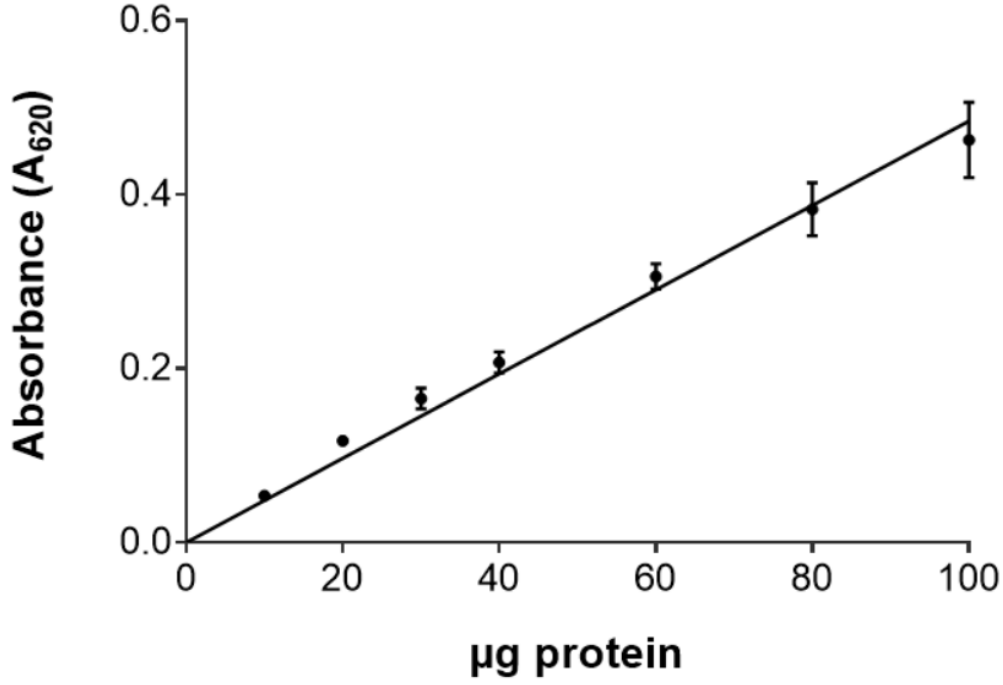

Figure 33. Standard curve for determination of protein concentration.
A standard curve for the assay had previously been made with an 80 mg/ml protein standard (5 parts bovine serum albumin and 3 parts IgG), diluted to 0.4 mg/ml. The diluted standard was used to make up seven samples of 250 µl containing 10 – 100 µg of protein. A blank sample, containing 0 µg of protein, was used to calibrate the instrument. The samples were incubated for 5-10 minutes at room temperature. Each sample was measured in triplicates. Mean absorbance of samples was plotted up against absolute amount of protein. y=0.0048x.

Sample preparation for stability measurements

Table B.1 Sample preparation for measurements on the effect of urea.
The table shows how the samples were prepared for the measurements on the effect of urea. Urea, buffer and enzyme were added from stock solutions. For variant G461A, final enzyme concentration was 0.02 mg/ml. For variant W460I, the final enzyme concentration was 0.07 mg/ml. Samples were incubated at 10°C overnight.

Sample	[urea] (M)	8.0 M urea (µl)	10x Mops buffer (µl)	Enzyme (µl]	H_2O (µl)
1	0.0	0	50	50	400
2	0.2	13	50	50	388
3	0.4	25	50	50	375
4	0.6	38	50	50	363
5	0.8	50	50	50	350
6	1.0	63	50	50	338
7	1.2	75	50	50	325
8	1.4	88	50	50	313
9	1.6	100	50	50	300
10	1.8	113	50	50	288
11	2.0	125	50	50	275
12	2.2	138	50	50	263
13	2.4	150	50	50	250
14	2.6	163	50	50	238
15	2.8	175	50	50	225
16	3.0	188	50	50	213
17	3.5	219	50	50	181
18	4.0	250	50	50	150
19	4.5	281	50	50	119
20	5.0	313	50	50	88

Absolute activity of variants after incubation in urea

Table B.2 Absolute activity of variants after incubation in urea

Mutants were subjected to various concentrations of urea. The samples' activity was determined with the standard activity assay (see section 2.6.1 for method description). The table shows mean activity with standard deviation (N=3).

Sample	[Urea] (M)	G461A activity (U/ml)	W460I activity (U/ml)
1	0.0	5.467 (1.414)	0.287 (0.026)
2	0.2	3.111 (0.236)	0.349 (0.008)
3	0.4	1.700 (0.186)	0.378 (0.034)
4	0.6	0.903 (0.023)	0.308 (0.039)
5	0.8	0.599 (0.019)	0.299 (0.055)
6	1.0	0.393 (0.066)	0.348 (0.017)
7	1.2	0.323 (0.011)	0.400 (0.011)
8	1.4	0.260 (0.026)	0.379 (0.046)
9	1.6	0.157 (0.016)	0.309 (0.005)
10	1.8	0.109 (0.035)	0.338 (0.014)
11	2.0	0.047 (0.010)	0.322 (0.018)
12	2.2	0.032 (0.020)	0.175 (0.016)
13	2.4	0.033 (0.024)	0.202 (0.022)
14	2.6		0.241 (0.046)
15	2.8		0.204 (0.020)
16	3.0		0.122 (0.009)
17	3.5		0.068 (0.012)
18	4.0		0.053 (0.003)
19	4.5		0.022 (0.008)
20	5.0		0.017 (0.007)

CD spectroscopy results

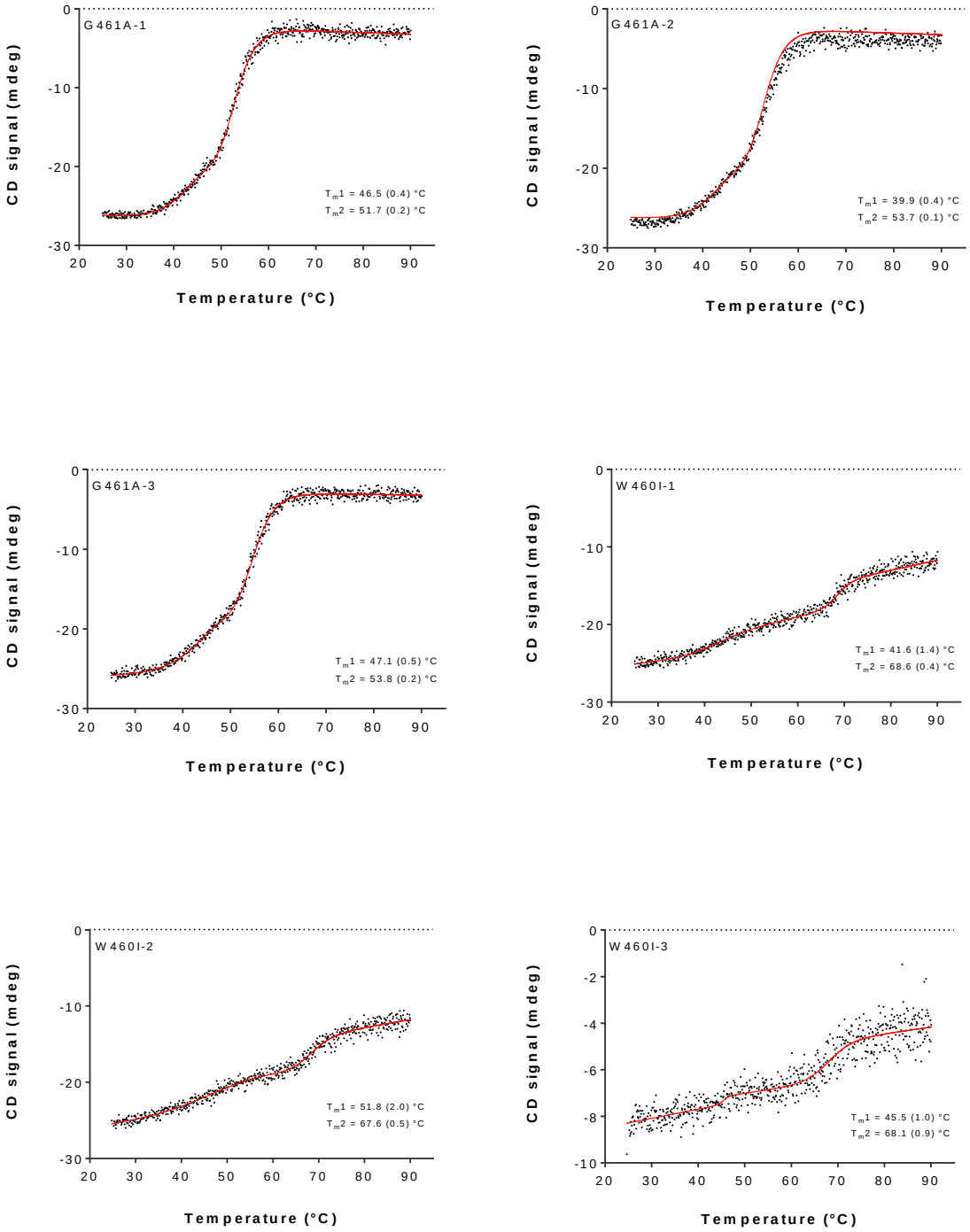

Figure 34. CD spectroscopy results of variants G461A and W460I.
CD spectroscopy was performed for three samples of each variant. The data was fitted to a three-state T_m function (CDpal© v.2.15) to determine melting points of the variants. Decreased CD signal of sample 3 is due to lesser protein concentration of the sample. Mean melting temperatures (with standard error) are: ***G461A:*** *T_m1 = 44.5 (1.3)°C, T_m2 = 53.1 (0.5)°C* ***W460I:*** *T_m1 = 46.3 (4.4)°C, T_m2 = 68.1 (1.8)°C*